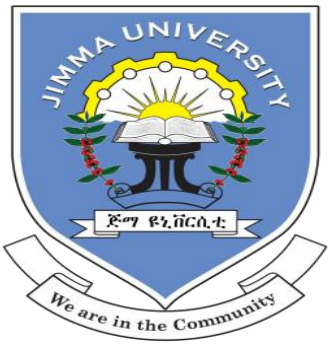

JIMMA UNIVERSITY

SCHOOL OF GRADUATE STUDIES

JIMMA INSTITUTE OF TECHNOLOGY

FACULTY OF MATERIALS SCIENCE AND ENGINEERING

CHAIR OF CERAMIC ENGINEERING

Investigations of the effect of Fe and Ni addition on the PbTe interfacial reactions

A Thesis Submitted to School of Graduate Studies of Jimma University in Partial Fulfilment of the Requirements for M.Sc. Degree in Ceramic Engineering

By

Chaltu Abebe Muse

November, 2020

Jimma, Ethiopia

JIMMA UNIVERSITY
SCHOOL OF GRADUATE STUDIES
JIMMA INSTITUTE OF TECHNOLOGY
FACULTY OF MATERIALS SCIENCE AND ENGINEERING
CHAIR OF CERAMIC ENGINEERING

Investigations of the effect of Fe and Ni addition on the PbTe interfacial reactions

A Thesis Submitted to School of Graduate Studies of Jimma University in Partial Fulfilment of the Requirements for M.Sc. Degree in Ceramic Engineering

By

Chaltu Abebe Muse

Advisor: DR. OLU EMMANUEL FEMI, Associate Professor ,Faculty of Materials Science and Engineering ,Jimma Institute of Technology ,Jimma University

November 2020
Jimma, Ethiopia

DECLARATION

I declare that this thesis has been composed by me and that the work has not been submitted for any other degree or professional qualification. Wherever contributions of others are involved, every effort is made to indicate this clearly with due reference to the literature and acknowledgement of collaborative research and discussions. The work has been done under the guidance of Dr. Olu Emanuel Femi and Dipanjan kumar. The experimental part of this research is conducted in Department of Materials Engineering, Indian Institute of Science, IISc, Bangalore, India, under supervision of Prof. Kamanio Chattopadhyay.

Name	**Signature**	**Date**
Chaltu Abebe Muse	_____	_____

Approved by advisor:

Advisor:

Name	**Signature**	**Date**
Dr .Olu Emanuel Femi(PhD)	_____	_____

ACKNOWLEDGEMENT

I would like to express my deepest appreciation to all those who provided me the possibility to do this work. For most, I would like to express my sincere gratitude to my advisor Dr.olu Emanuel Femi, whose contribution in stimulating suggestions and encouragement helped me to coordinate my thesis. I would also like to acknowledge my university Jimma institute of science and technology (JIT) for providing me the financial support to do my research work. Furthermore I would like to acknowledge with much appreciation the crucial role of the Prof. Kamanio Chattopadhyay and Indian Institute of Science, IISc who gave the permission to use all required equipment and the necessary materials to do the experimental work.

A special thank you goes to the staff members in the materials engineering in Indian institute of science, especially my advisor Dipanjan Kumar who helped me on the preparation and analyses of samples.

I thank my fellow lab mates and my friends for the stimulating discussions, working together and for all the fun we have had.

Last but not least, I would like to thank my family; my father Abebe Muse, my mother Dinke Oljira and my two sisters Lensa and Horiyan who have always believed in my capabilities to finalise this incredible achievement and supporting me spiritually throughout my life.

Abstract

PbTe based thermoelectric generators are widely employed by the United States Army in space crafts to supply on-board power, and in pacemakers batteries, it's one among the widely used thermoelectric semiconductor material with good chemical stability, good mechanical strength, high melting point, low vapour pressure, and intermediate operating temperature (900 K). But still, the PbTe module suffers from low efficiency, and comparatively research on thermoelectric modules is at a primary stage because of the gap between the material and device technologies. Thermoelectric devices are composed of different layers, such as electrodes, insulators, thermoelectric elements, and bonding interfaces. These layers have different physical features, and to construct thermo mechanically reliable devices. The interfacial reaction between the electrode and the thermoelectric leg has to be considered. Ni and Fe are commonly used as a diffusion barrier and electrode for PbTe because the mismatch of coefficient of thermal expansion is very low comparing with the other materials.in the case of metallization of PbTe with Ni, it was observed that both Ni-Te intermetallic and voids can form near the bonding interface which can lead to high electrical and thermal contact resistance. It is also difficult to get a metallurgical high strength joint with Fe. Fe can only bond at a high temperature which can affect the property of thermoelectric leg PbTe. We have added the atomic present of Fe to Ni to investigate the Effect of Fe addition (Ni-at1%, 2at%, 5at %) in the PbTe/Ni interfacial reaction, and we observed promising results. The experiment is undertaken at different temperatures and time intervals to study the kinetics and based on our results we conclude that Ni-5at%Fe /PbTe 700^{o}C/15min is the best one, if we increase beyond 5at%Fe it would take a longer time to join. The detailed results will be described in chapter 4 of this thesis.

Contents

List of Figures

List of Tables

Chapter one

1. Introduction

Thermoelectric technology that converts heat into electrical energy or vice versa enables clean and sustainable power generation[1] because it does not involve any moving parts nor does it release any by-products into the environment. Thermoelectric generators (TEG) can be applied for example in the direct conversion of geothermal or solar energy into an electric one, they can also play a major role in recollecting waste heat produced in-car internal combustion engines or industrial installations. Therefore, thermo power generation is believed to be among key technologies that will allow the harnessing of a large amount of waste heat produced, however, thermoelectric generators suffer from low-conversion efficiency[2], even though significant progress has been attained in the development of high-efficiency thermoelectric compounds, the development of thermoelectric modules to take advantage of these materials has not been rapid so far[3], only low temperature (<200) thermoelectric materials such as Bi_2Te_3-based alloys, have been widely developed and incorporated in commercial cooling or heating devices[7]–[10].

The development of an efficient thermoelectric generator (TEG) requires the fulfilment of several factors, which include the availability of n-and p-type thermoelectric materials with high figure -of merit (ZT), preparation of ohmic contacts between thermo elements and metallic interconnects and management of maximum heat transfer through the device. Beyond thermoelectric materials, the device concept needs to be aggressively addressed before thermoelectric generators can be intended as power sources[8].In this thesis, we are focusing on the PbTe based thermoelectric module and effect of Fe addition (Ni-at1%, 2at%, 5at%Fe) in PbTe/Ni interfacial reaction.

1.1 Thermoelectric properties and parameters

1.1.1Seebeck effects

Seebeck effect is the most fundamental thermoelectric phenomena[9]–[12]. In the early 1800s Seebeck observed that when two dissimilar materials are joined together and the junction is held at different temperatures (T and T+ΔT), a voltage difference (ΔV) develops that is proportional to the temperature difference (ΔT)[13]. The ratio of the voltage developed to the temperature gradient (equation 1.2) is related to an intrinsic property of the materials called Seebeck coefficient α. The relationship is given as in equation in terms of conventional

current (I), the individual Seebeck coefficient of materials, and electrical resistance (R) as follows;

$$I = \frac{((T+\Delta T)-T)(\alpha_P-\alpha_n)}{R} = \frac{\Delta T\alpha}{R} \quad \text{..... (1.1)}$$

$$\alpha = \Delta V/\Delta T \quad \text{..... (1.2)}$$

Where V is the voltage, T is the temperature. The Seebeck effect results from the diffusion of charge carriers from the hot side to the cold side in the thermoelectric material due to the charge carriers having higher thermal energy on the hot side compared to the cold. The Seebeck coefficient of the materials mainly depends on their electron band structure which depends on the density of state (DOS) in the range of Fermi level[14]. A high DOS and medium carrier concentration produce a large Seebeck coefficient. The Seebeck coefficient is very low for metals (only a few microvolts per degree kelvin) and is much higher for semiconductors (typically a few hundred microvolts per degree kelvin).

1.1.2 Peltier effect

Peltier effect: was discovered a few years later by Peltier, who observed that when an electric current is passed through the junction of two dissimilar materials, heat is either absorbed or rejected at the junction, counting on the direction of the current. The Peltier coefficient $\prod$ is defined as the ratio of the rate of heating or cooling to electrical current passing through the junction and is expressed as;

$$\prod = \alpha T \quad \text{.....(1.3)}$$

later in 1855, W. Thomson recognized the mutual dependency of the two effects through the first Kelvin relation[15], [16] as given in (equation 1.4).

$$\frac{d\prod}{dT} = K_{kelvin}+\alpha \quad \text{.....(1,4)}$$

whereK_{Kelvin} is the kelvin constant and $\prod$ is the Peltier coefficient. Peltier and Seebeck's coefficients are related by fundamental relationship, which is given by $\prod = \alpha T$. The Fermi energy of the two conductors can be used to describe this phenomenon.

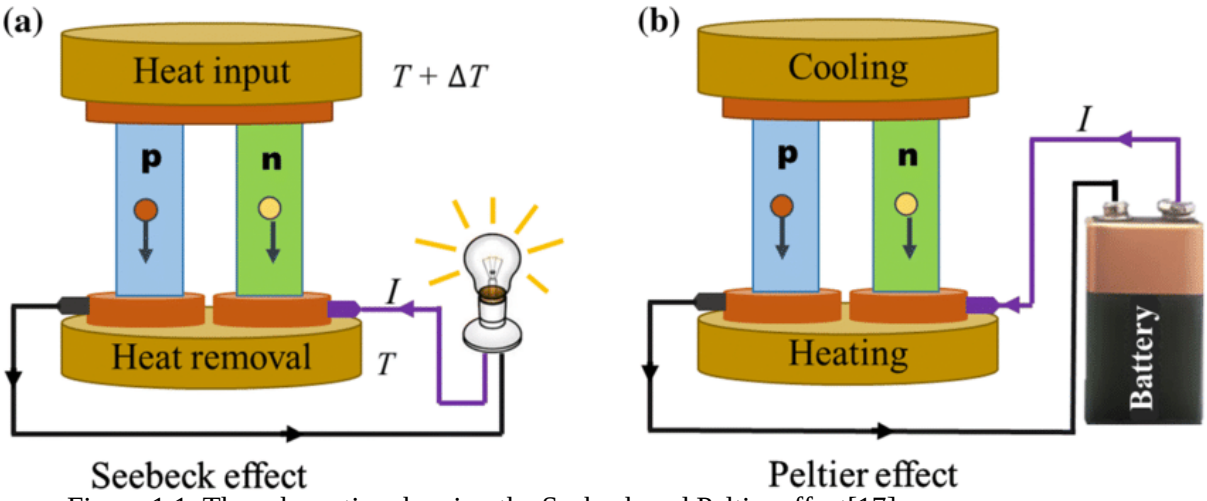

Figure 1.1. The schematics showing the Seebeck and Peltier effect[17].

1.1.3 Thomson effect

Thomson effect is the absorption or evolution of heat when current is passed through an unequally heated conductor and the Thomson coefficient is defined as the electromotive force set up between the two points of a conductor which has a temperature difference of 1^{o}c. It is defined by σ.

$$\sigma = dv/d\theta \quad \text{.....(1.5)}$$

Where dv= potential difference set up between two points of the conductor

dθ = temperature difference between those points.

1.1.4 Electrical conductivity

A good thermoelectric material must exhibit high electrical conductivity (σ), and ohm's law as the following equation demonstrates its relationship to the electric current (I) and voltage (V).

$$I = \frac{\sigma V A}{L} \quad \text{..... (1.6)}$$

Here, A is area and L is the length of the sample. The type and concentration of the charge carrier involved mainly govern electrical transport properties.

1.1.5 Thermal conductivity

Electric thermal conductivity (k_{el})and lattice thermal conductivity(k_{ph}) are the two-heat transport in a material given by the Wiedemann- Franz law;[18]

$$\kappa = \kappa el + \kappa ph \quad \text{..... (1.7)}$$

$$\kappa el = \sigma TL \text{ .... (1.8)}$$

Where; κel and κph are the electronic and phonon thermal conductivity respectively and L is the Lorenz.

To increase the figure of merit (ZT), the σ/k value must be maximized, therefor; kph should be reduced.

1.2. Optimization of thermoelectric materials

1.2.1 Figure of merit

The maximum efficiency of a thermoelectric device for both thermoelectric power generation and cooling is determined by the dimensionless figure- of- merit, ZT[19]–[23].

$$ZT = \frac{S^2\sigma}{k}T \text{ .... (1.9)}$$

Where S is Seebeck coefficient, σ is electrical conductivity, and $k = k_p + k_e$ is the thermal conductivity which is composed of the lattice (photonic) thermal conductivity k_p and electronic thermal conductivity k_e. All these parameters are a function of carrier concentration. the precise carrier concentration to maximize ZT depends on temperature and the specific semiconductor[24]. It is difficult to increase the electrical conduction of the material by increasing the carrier concentration to maximize ZT without affecting the other parameters.

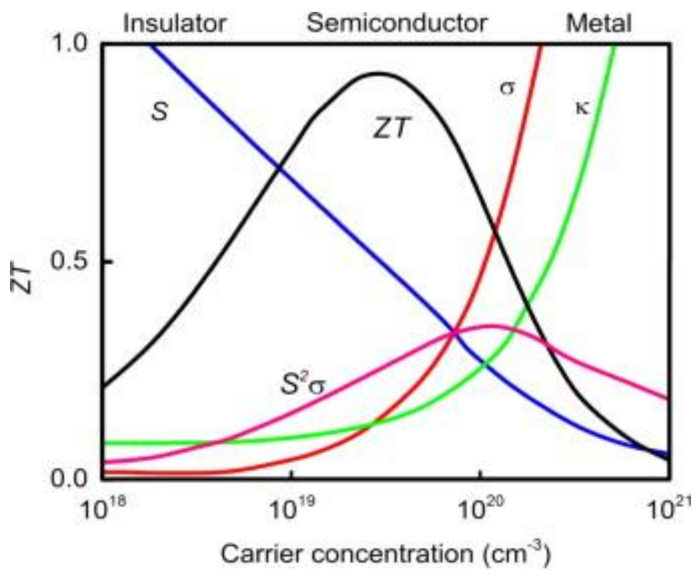

Figure 1.2. Plot showing the mutual dependency of the TE transport properties on the electronic charge carrier concentration, n [25].

In thermodynamics the foundation theory of heat recovery is that waste heat has a lower value higher entropy, a lower energy) than other forms of energy. The highest theoretical efficiency a heat recovery system can obtain is given by Carnot efficiency;

$$\eta_c=(T_h-T_c)/T_h \quad \text{(1.10)}$$

Where; T_h is the temperature of hot side, T_c is the temperature of cold side.

1.2.2 Thermoelectric materials

A good thermoelectric material should have electric conductivity of a crystalline material and thermal conductivity of an amorphous or glass-like material[26]–[32]. High-performance thermoelectric materials that have high ZT and can operate with a broader temperature regime (especially T > 500K) have been pursued, since Bi_2Te_3 – based alloys were discovered in the 1960s. progress had been made in the development of TE materials by two different research approaches one by exploring new materials with complex crystalline structures, and the other by reducing the dimension of the materials[33]–[39].

Research for synthesizing new thermoelectric material is focused to tune the lattice part of thermal conductivity to a minimum. This is achieved by scattering phonons by different methods like mass fluctuation scattering, rattling scattering, grain boundary scattering, and interface scattering. Thermoelectric materials are typically classified by material structure and composition. Some of the main classifications are non-oxides (chalcogenide, clathrate, skutterudite, half-Heusler, silicide) and oxides[40], [41]. Metal oxides have recently attracted

much attention as thermoelectric power generation materials at high temperatures supported their potential advantages over heavy metallic alloys in chemical and thermal robustness. oxides were believed to be poor thermoelectric materials because of the low carrier mobility arising from the weak orbital overlap and localized electrons until the discoveries of good p-type thermoelectric in layered cobaltite's $NaCo_2O_4$ 75, $Ca_4Co_3o_9$ 76 and $Bi_2Sr_2Co_2O_9$ 77 with large Seebeck coefficients, low thermal conductivities (<1W/mK) and ZT ≈ 1 at 700 – 1000 k[42]. The most promising candidates for n-type oxide thermoelectric materials include perovskite-type $SrTiO_3$ and $CaMnO_3$-δ.

A chalcogenide is a chemical compound commonly used for tellurides, selenides, and sulphides. It consists of at least one chalcogen anion and one more electropositive element. Chalcogenide materials have a long history of demonstrated thermoelectric use with bismuth telluride and lead telluride being the most prominent[43]–[46]. Lead telluride has better thermoelectric properties at higher temperatures (500 - 600^{O}C). PbTe contains heavy elements, which lead to small phonon group velocity and low thermal conductivity. Such heavy elements usually have small bandgaps and large mobility. PbTe-based thermoelectric generators have been used in several NASA space missions, from Transit 4 A to Viking 2, and in the Mars rover Curiosity. PbTe is a semiconductor with a direct bandgap of 0.32 eV and a highly symmetric crystal structure which is the opposite of a complex crystal structure. In part, its relatively low lattice thermal conductivity of 2.2 W m–1K–1stems from its very high average molar mass of 167.4 g mol–1. A re-investigation of the properties of the historic n-type PbTe revealed ZT values ≈1.4 between 700 K and 850 K[47]. Introducing Nano domains caused a significant performance increase as reflected in a ZT max= 2.2 at 800 K for co-doped $AgPb_{18}SbTe_{20}$[48], [49] forming solid solutions in PbTe based materials can reduce lattice thermal conductivity and engineer the band structure to enhance the electrical properties.in quaternary alloys of $Pb_{1-x}Mg_xTe_{0.8}Se_{0.2}$, The significant roles of MgTe in enhancing electrical properties and reducing the thermal conductivity of $PbTe_{0.8}Se_{0.2}$ were investigated and a maximum *ZT* of ∼2.2 at 820 K was achieved in $PbTe_{0.8}Se_{0.2}$ with 8% MgTe[50]. Bi_2Te_3 is commonly used in TE material for cooling applications. Its structure consists of closest packed layers of the cations and anions, but with a more complex order of...Te-Bi-Te-Bi-Te.... As a consequence, its transport properties are isotropic, meaning the thermoelectric performance depends on the direction of the heat and electron flow. It's a narrow-gap semiconductor, with 0.16 eV, and a melting point of 858 K[51]. Co-doping with

the transition metal atoms Cu, Ag, and Cd gave ZT max= 1.4 at 425 K[52]. The Bi_2Te_3/Sb_2Te_3 super lattices with ZT max= 2.4 is reported[53].

Skutterudites are chased by many researchers for potential power generation applications in the mid (500 – 900K) temperature range[54]–[57]. The crystal formula of skutterudites can be written in MX3 where M is Co, Rh or Ir, and X is P, As or Sb[58]–[60]. The key feature is a large space. In $CoSb_3$ each unit cell contains eight pseudo cubes formed by Co and Six squares formed by Sb[42]. The voids can be filled by different elements such as rare- earth, alkaline -earth, or other heavy atoms. Lattice thermal conductivity of rare- earth-filled skutterudites $Ir_4LaGe_3Sb_9$, $Ir_4NdGe_3Sb_9$, and $Ir_4SmGe_3Sb_9$ were stated to be over an order of magnitude lower than the unfilled $IrSb_3$[61]–[63].The phonon -electron scattering in the case of Nd3+ and Sm3+ helped reduce lattice thermal conductivity, but the electronic properties also degraded. Progress with p-type skutterudites has been slower since filling tends to drive skutterudites' strong n-type.

Clathrates are another class of compounds that can be classified into two types, type 1 and type 2, they have open structures to host loosely bounded atoms[64]–[66]. Clathrates have a $_{large}$ number of atoms in the unit $_{cell}$ and low thermal conductivity. Type 1 clathrates can be represented by $X_2Y_6E_{46}$ and type 2 is represented by $X_8Y_{16}E_{136}$ where X and Y are guest atoms, they can be alkali, alkaline earth, or rare earth metals and E refers to a group 14 elements (Si, Ge, Sn…). clathrates can possess a glass-like structure to indicate that this system is a phonon glass electron crystal system which makes it interesting for thermoelectric application[30]. Engineering of clathrate and skutterudites has involved the introduction of guest atoms into a base structure. These additions can optimize electron concentration or act as phonon scattering sites. Such materials engineering to achieve a glass-like thermal conductivity combined with good charge carrier mobility has been termed the “phonon glass electron crystal” approach. With one vacant sub lattice in the crystal structure, the properties of half-Heusler materials have also been improved through void-filling as doping of the filled sub lattices.

Half-Heusler is a relatively new topic, and they have gained ever-increasing attention as promising high-temperature thermoelectric materials. Half -Heusler compounds have a cubic structure consisting of three interpenetrating FCC sub lattice and one vacant sub lattice, their chemical composition is XYZ, where X is a transition metal, a Nobel metal or a rare earth element, Y is a transition metal or noble metal and Z is the main element, mostly P -

block[67]. They have good properties such as high thermal stability and environmental friendliness. They exhibit promising power factors when properly doped. Half-Heusler compounds typically have a relatively high lattice thermal conductivity, by alloying and Nano structuring the lattice thermal conductivity can be reduced. MNiSn (n-type) and MCoSb (p-type) are mostly focused half-Heusler materials[68]–[70]. There is only limited research on half- Heusler materials and devices, especially on the interfacial structure between the metal electrode and HH compounds for device application.

1.3. Thermoelectric module

The thermoelectric module is fabricated as a set of thermocouples whereby each thermocouple has one leg of p-and one of n-type thermoelectric material, with dimensions of few millimetres, which are connected electrically in series but thermally in parallel. The efficiency and reliability of the thermoelectric device are two important issues for device design[71]. Even though significant progress has been attained in the development of high-efficiency thermoelectric materials, thermoelectric devices have been limited to low temperatures. TEG not only bases its performance efficiency on the dimensionless figure of merit (ZT) of p and n couples but also on good contact with the electrode. Therefore, not only the physical properties of the p- and n-semiconductor have to be taken into consideration. But also, the properties of the metal-semiconductor interface, especially their stability, electrical and thermal resistance are important.

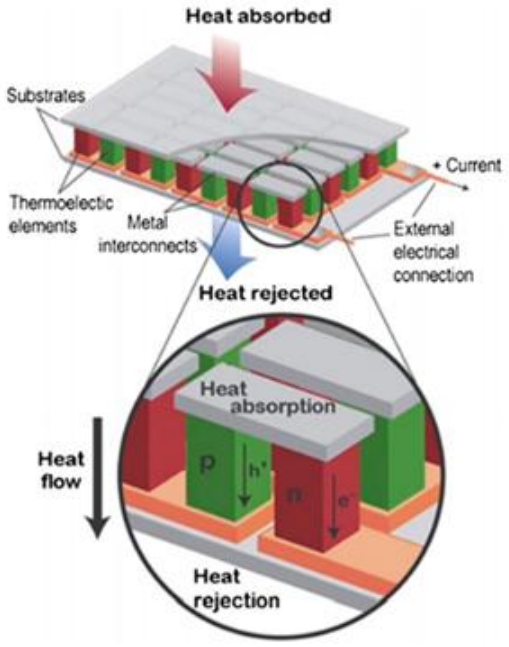

Figure 1.3. Working principles of thermoelectric module [72].

As a function of hot side (Th)and cold side (Tc) temperature the module efficiency can be expressed by; [72]

$$\eta\max = \frac{Th-Tc}{Th}\frac{\sqrt{1+ZT}}{\sqrt{1+ZT}}\frac{-1}{+\frac{Tc}{Th}} \quad \text{..... (1.11)}$$

A cascade and segmented TEG have been developed for high-efficiency energy conversion.

Segmented TEGs are made up of of two or more layers of TE materials arranged in series. Cascaded TEG has two or three stages and it is used in the energy recovery of high-temperature waste heat, which is applicable in many industries. Segmentation, allows TEGs to operate in a larger thermal gradient and provide higher output power and efficiency compared to the non-segmented TEGs under the same thermal gradient. Hu et al. reported that a segmented TEG module constructed using nanostructured PbTe- and BiTe-based materials had an efficiency of 11% at a temperature difference of 590 K, as compared to the efficiency of 8.8% from a non-segmented TEG module made using just nanostructured PbTe material[73].In both segmented and cascaded TEG, the incompatible thermoelectric materials can decrease efficiency. Segmentation presents additional thermal and electrical interfaces between different TE layers, which increases contact resistance. The electrical contact resistance generates extra Joule heat and the thermal resistance leads to a sudden temperature drop at the interface. Both these effects can affect the performance of TEGs. The performance of TEGs not only depends on the ZT of TE materials but also on the arrangement of the TEG modules. Geometric parameters such as length, width, and height of p-n legs, the gap distance between legs, operating conditions such as hot-side and cold-side temperatures, and energy losses due to convection and radiation, collectively affect the performance of TEGs.[74]

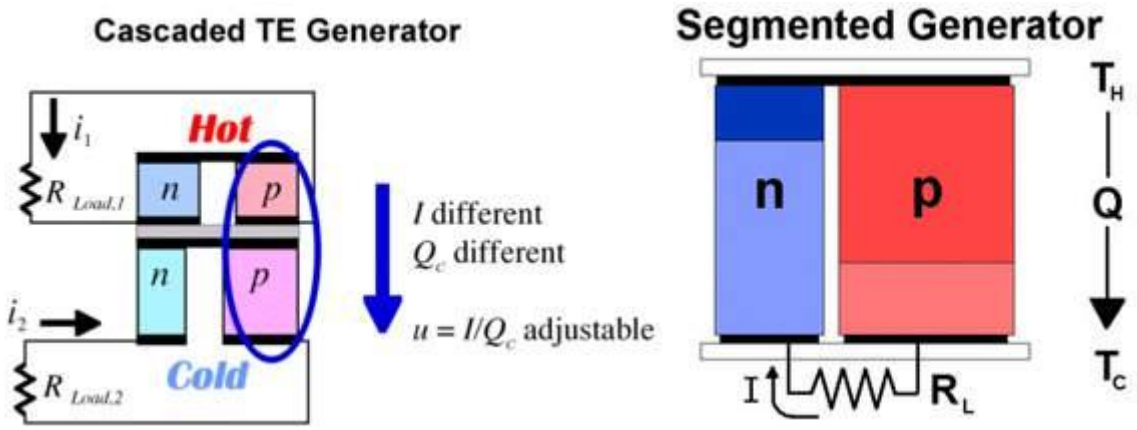

Figure1.4. A cascade and segmented[75]

1.4 Diffusion in solids

In material science, we are interested in controlling microstructures. Reaction or microstructural changes in solids, take place through the movement and transport of atoms in the solid phase, and phase transformation often involves diffusion. Diffusion is a mass transfer from a region of high concentration to a region of lower concentration[76]. It takes place in all forms of matter; but it is relatively fast in gas because the gas molecules have greater kinetic energy, slow in liquid, and very slow in solids. The main driving force behind this phenomenon is the concentration gradient. Additionally; diffusion species, temperature, stress, solubility, defects, etc also play their role. Diffusion is an isotropic process, i.e. it does not have a preferred direction in most solid such as in glass materials (amorphous) and crystalline materials, however; in an anisotropic material, diffusion depends on specific direction i.e. as in a non-cubic crystal. Diffusion takes place by moving step by step of atoms from one lattice site to another. For this to happen there has to be an empty site and sufficient energy to break the bond with neighbours. To break the bond atoms, get energy from atomic vibration (small-amplitude vibrations about their equilibrium positions), temperature increases such vibrations and at any temperature, a very small fraction of atoms has sufficient amplitude to move from one position to another position.

For a particle or atom to move from one crystal point to another in a specific crystal lattice, there must be a defect, which allows the particle's movement. Point defects, vacancies, and interstitial ions are responsible for lattice diffusion. Diffusion also takes place along line and dislocations, external surface defects which include grain boundaries which provide a much faster path for atomic movement. Grain boundary and dislocation diffusion are generally faster than bulk or lattice diffusion.

1.4.1 Phenomenological descriptions of diffusion

Fick's first law

Diffusional flux is equal to negative concentration gradient times constant factor (diffusion coefficient)[77].

$$J = - D\ (dc/dx) \quad \text{......} (2.1)$$

The negative sign shows diffusion taking place from higher concentration to lower concentration. It indicates that J is positive when movement is down the gradient, and the negative cancels the negative gradient along the direction of positive flux.

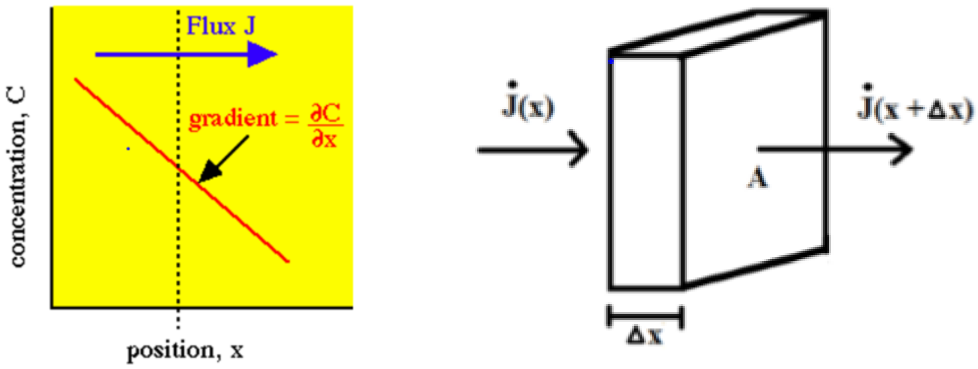

Figure 1.5. Schematics showing the diffusion flux (J) is the diffusion flux ($cm^{-1}s^{-1}$) it measures the amount of matter that flows through a unit area during a unit time interval, D is the diffusion or diffusivity, c and x is the concentration (amount of substance per unit area) and position (length) respectively[78].

Fick's second law

For non- steady-state processes this law can be derived from Fick's first law and it relates to change of concentration with time and change of concentration with the position.

$$dc/dt = d/dx\ (D\ dc/dx) \quad \text{......} (2.2)$$

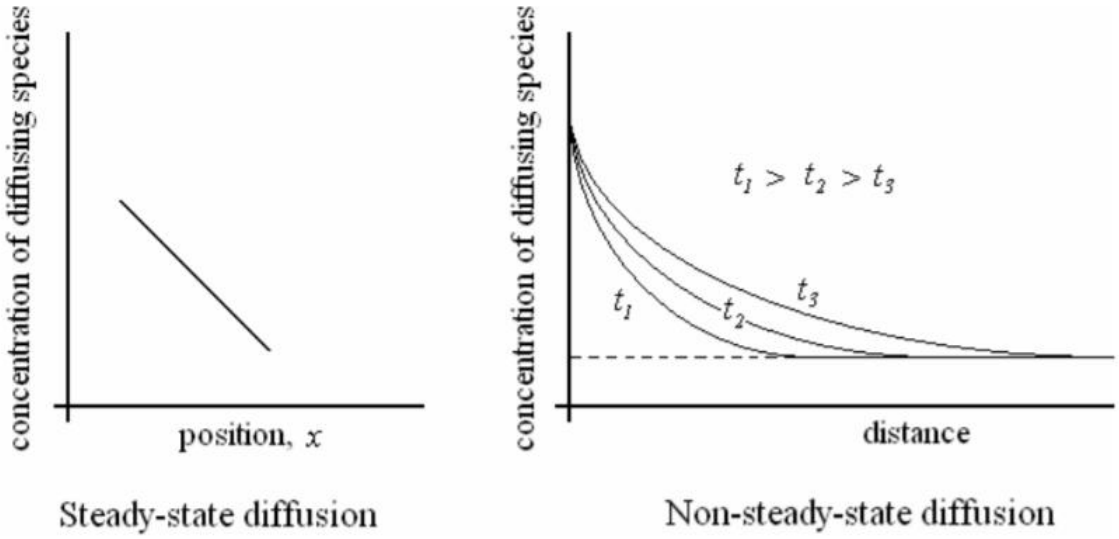

Figure 1.6. steady- state diffution and non steady – state diffusion[79]

Fick's first law applies to a steady-state system, where concentration keeps constant with time. However, in many cases, the concentration changes with time, the Fick's second law describes the diffusion kinetics in these cases. It gives us the range at which concentration is changing at any given point in space and it takes the form of a partial differential equation.

1.4.2 Diffusion mechanisms

There are different types of diffusion mechanisms. some of these include; vacancy, interstitial, ring, and interstitially diffusion[80], [81]. Generally, Vacancy (substitutional) diffusion and interstitial diffusion are two basic solid-state diffusion mechanism[82], [83]. Vacancy diffusion happens when atoms move from a normal site to an adjacent unoccupied lattice site if an energy barrier between the two positions is recovered. This energy can be provided through thermal agitation. In another way, interstitial diffusion is a diffusion of the solute atom which is small enough to occupy interstitial site jump from one interstitial site to a neighbouring site. Interstitial diffusion is faster than vacancy diffusion as only small activation energy is required for an interstitial atom to move.

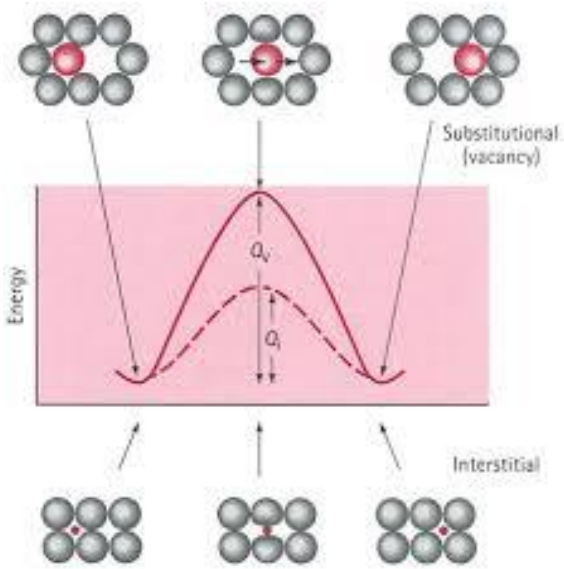

Figure 1.7. Illustrations of substitution and interstitial diffusion*[84]*

1.4.3 Diffusion path

Both the interstitial and vacancy diffusion take place inside the lattice therefore it is called lattice diffusion. Atoms can also present on the free surface of a crystal and during crystal growth, the new atoms which are coming will always join the surface and they will move along that surface so it is possible for an atom to sitting on the surface to move to the next neighbouring site on the surface it can be called surface diffusion. Or an atom can diffuse along the grain boundary, The regions around the grain boundary is not tightly packed as a region inside the grain, therefore, there is more open space along the grain boundary and an atom can sit in those open spaces and an atom can present at the grain boundary and it may jump from one-grain boundary site to the other grain boundary site. Diffusion along dislocation is also possible when a defect is present.

1.4.4 Factors that influence diffusion

Diffusion can be affected by different factors such as; temperature size of diffusing species, density, lattice structure, and presence of defects. Temperature is the most known factor that influences the rate of diffusion[85]. As temperature increases diffusion rate also increases and lowering the temperature will lower the diffusion rate. When the temperature is increased kinetic energy of each particle is increased that leads to an increase in velocity, which means there is a greater possibility of collisions between particles which increases the rate of diffusion. high density (region of a greater number of the particle) results in an increased rate of diffusion. The region with a lower number of particles has a low chance of collision (low rate of diffusion). Diffusion is faster in open lattice than closed lattice or direction. Presence

of defects; like dislocation, grain can also boundaries enhance the diffusivity of diffusing species.

1.5 Background of the study

Although some researchers have designed and fabricated some TEG modules with high output power there is no reliable TEG module in the commercial markets. The challenges to commercialization arise mainly from several factors such as a low thermoelectric (TE) conversion efficiency, poor mechanical properties and thermal stability of TE material, unreliable contact between TE legs and electrodes, high production cost, and so on. The low reliability of TEG modules at high service temperatures has become a factor limiting the wide application of TEG technology. It is well known that the TEG module consists of an alumina ceramic plate, electrodes, a solder layer, an anti-diffusion layer, and TE legs[86], [87]. The reliability of a TEG module is closely related to the connection process at the high-temperature side. For the traditional TEG module, copper flow deflectors are often used as electrodes, and the TE legs are connected to the copper electrodes at the hot side by soldering technology. Nevertheless, the mismatch between the thermal expansion coefficients of the copper electrodes and TE materials greatly reduces the service life of TEG modules. At the same time, the interfacial reaction and elemental diffusion between the copper electrodes and TE materials also degrade the TE properties of the TEG module. In terms of their key materials thermoelectric module can have four parts;(1) thermoelectric conversion materials (TFcM) or we can call thermoelectric leg, and it converts energy (2) thermoelectric interface materials (TEiM) that is used in maintaining the reliable and low energy loss transport of heat and electricity between electrode strip and TEcM, (3) package material, used to prevent the evaporation of the TEcM and thermal insulation, (4) housing materials, providing support and electrical insulation. Additionally, solder or brazing materials and electrode stripes are also necessary for a TEG module. Most efforts have been done on searching efficient TEcM for the past years among the four key materials. However, the TEiM and the interface with TEcM are still a challenge when we assemble a thermoelectric power generation module.

This thesis is part of an effort to explore the thermoelectric contact material (diffusion barrier) specifically for the PbTe based thermoelectric module

1.6 Statement of the problem, scope, and objectives

1.6.1 Statement of the problem

Since Seebeck discovered voltage generation, which is almost around 200 years ago scientists

have been trying to improve the ZT of known materials or searching for new materials. Novel materials with an outstanding combination of high electrical and Seebeck coefficient as well as low thermal conductivity is very much desirable for any thermoelectric application and progress has been attained in the development of high-efficiency thermoelectric compounds, but the development of thermoelectric modules to take advantage of these materials and commercializing was very slow. PbTe -is one of the thermoelectric materials that are good candidates for harvesting waste heat at mid-range temperatures. Integration of PbTe in TE devices has a significant impact on the conversion efficiency, PbTe-based TE materials may be more difficult to be bonded with electrodes because the CTE of PbTe-based TE materials is about 20×10^{-6}/K, which is much higher than most of the refractory metals commonly used as diffusion barriers or electrodes and diffusion of electrode/solder materials into thermoelectric legs, Inter-metallics formed during fabrication are an issue. People have done studies on Ni /PbTe interface by hot pressing and spark plasma sintering technique and PbTe can rapidly react with Ni to form the beta phase and liquid Pb at 600^{o}c. Therefore, in this work, we aim to produce a new diffusion barrier for PbTe based thermoelectric material by using a diffusion bonding technique and investigate their thermoelectric response and performance

1.6.2 Scope

This work includes investigation of the Effect of Fe and Ni in PbTe interfacial reaction. It does not include the fabrication of a thermoelectric device design at this particular stage and the transport property of thermoelectric material is also not investigated.

1.6.3 General Objective

The objective of this study is to develop effective and reliable Ni-Fe/PbTe based thermoelectric joints at high temperatures.

1.6.4 Specific objectives

- Developing alternative approaches for bonding metallic contact to PbTe thermoelectric leg
- Finding an effective bonding layer/ diffusion barrier for PbTe based module
- Synthesis of PbTe and Ni-Fe
- Coupling and sealing of PbTe and Ni-Fe
- Characterizations of the diffusion couples

Chapter Two

2. Literature reviews

2.1 Recent developments in thermoelectric contacts

2.1.1 Interface

Recent studies in thermoelectric generators focus on the challenge at the interface of the thermoelectric leg and the diffusion barrier layer [88]–[92]. The efficiency of some thermoelectric devices is also improved following the development of structural design and joining techniques [73], [93]–[95]. An interface is responsible for transferring heat, electricity, and force [43]–[45]. In the thermoelectric module joining the electrode and thermoelectric element is important. Soldering and brazing have been applied in traditional thermoelectric devices. But, poor solderable capability and high electrical sensitiveness to solder was a challenge .it is realized that the metallization technique is more significant. Generally, in the thermoelectric module to develop good thermoelectric barrier layer/thermoelectric leg interface, at least the following requirements have to meet; high bonding strength, high chemical and thermal conductivity, and low contact thermal and electrical resistivity.

2.1.2 Bonding strength

Commercially available thermoelectric devices show mechanical failures after thermal cycles and aging this is because of the thermal stress. Global thermal stress and local thermal stress are two stresses which take place as a result of the expansion difference of the electrodes between the hot side and cold side, and the expansion difference of thermoelectric barrier material and thermoelectric conversion material respectively. Ziabari et al, [96]suggest that using thinner and longer legs the global stress in a module can be reduced. In bonding strength, two factors are very important the first one is surface roughness due to anchor effect and it was done by chemical etching and sandblasting. Weitzman et al. [97] applied an etching solution (nitric acid: hydrofluoric acid: glacial acetic acid) for the p-type Bi_2Te_3 while another solution (nitric acid: hydrochloric acid) for the n-type Bi_2Te_3. The other one is surface cleaning and it reduces the contact resistivity and also removes the surface oxides. Talor et al [98]involved the plasma cleaning in the $(Bi_2Sb)_2(Te, Se)_3$ system and reported 10^{-4} Ωcm^{-2} to 10-6 Ωcm^{-2} contact resistivity reduction.

2.1.3 Interfacial thermal resistance

The acoustic mismatch model (AMM) and the Diffusive mismatch model (DMM) are the two different models that are known to explain interfacial thermal resistance. Khalatnikov [99] proposed the AMM theory and he assumed that phonons are plane waves, the interfaces are perfect planar and the materials are continua. Swartz and Pohl presented an opposite idea [100] they believed that all the incident phonons are diffusely scattered at the interface and diffuse scattering at the interfaces destroys the phonon corrections. The modern Molecular Dynamic (MD) simulation explained that at the interface phonons can be scattered in the way of acoustic scattering and diffusive scattering. In the interface, the roughness of the material, oxidation gas absorption, and applied pressure can also be a problem. The intrinsic physical properties are more important for a good bonding interface. Interfacial thermal resistance decrease with increasing temperature and the interfacial thermal resistance of a good bonding interface is lower than the loos contact interface.

2.1.4 Interfacial electrical resistance

W. Schottky, F. Braun, A.H. Wilson, N. F. Mott, A.H. Bethe, etc [101]described the electrical transport behaviour of the metal-semiconductor interface. The interfacial electrical resistance is identified by a potential barrier and the contact distance gap in the non-diffusion interface. In the metal-semiconductor interface, the contact distance gap δ results in a tunnelling potential barrier and the tunnelling potential barrier decline to zero with the decreasing gap δ. Schottky potential barrier (φ_B) is resulted from the surface electron transfer due to the work function difference between the metal and the semiconductor. $\phi_{SPB} = \phi_m - \phi_{s,n}$ *for* n-type semiconductor and $\phi_{SPB} = \phi_{s,p} - \phi_m$ for p-type semiconductor. To achieve an ohmic contact the band alignment should meet the condition of $\phi_m < \phi_{s,n}$ for the n-type while, $\phi_m > \phi_{s,p}$ for the p-type semiconductor.

2.1.5 Stability

The long-time service of the thermoelectric device is one of the factors that have to be considered. Therefore, the stability of the thermoelectric interface material /thermoelectric leg interface plays an indispensable role in the thermoelectric module. Diffusion-controlled stability and reaction-controlled stability can describe interface stability. Diffusion controlled stability involves atomic diffusion at the interface. Even though diffusion is necessary for having strong bonding of the thermoelectric leg/diffusion barrier layer interface especially during the joining process. Diffusion during the service time can deteriorate the device performance and reliability, then shorten lifetime because thermoelectric transport properties

can be significantly changed by the doping effect of diffusion. On the other hand, reaction-controlled stability is characterized by new phase formation. The interfacial reaction takes place during the diffusion of atoms from both sides of the interface materials which can result in reducing the thermoelectric performance and stability. Ni/Bi_2Te_3 is one of the commercially available devices, some of the intermetallic compounds such as Ni_2Te_3, NiTe are observed at high temperatures this can also cause a high concentration of Te vacancy can shift the thermoelectric conversion material from the optimized carrier concentration range and also weakens the mechanical bonding strength.

2.1.6 Design principles for thermoelectric interface material

The mismatch of the coefficient of thermal expansion (CTE) between the thermoelectric interface material (TEiM) and thermoelectric conversion material (TEcM) can lead to an interface crack during the joining process when high temperature is applied. This can influence the bonding strength and stability of the interface. Therefore, matching or reducing the mismatch of the CTE is very crucial. Theoretically thin and ductile thermoelectric interface material layer is suggested. The work function of the material is also important. The Schottky potential barrier is one of the controlling events in electrical contact resistivity. The contact resistance has to be less than 5 $\mu\Omega cm^{2.}$ Work function mismatch can be reduced by doping layer at the semiconductor side. Diffusion passivation and dopant inactive principle are the other factors to be considered, doping is used in TEcM to adjust carrier concentration however it can cause some changes like increasing interface electrical resistivity due to diffusion, and therefore it is important to consider the dopant or doping element for TEiM. The easy bonding process principle is also necessary. There are different bonding processes such as hot pressing, spark plasma sintering (SPS), electrochemical deposition, chemical vapor deposition, etc. These processes can have an impact on the interface resistance and bonding strength. Generally, in developing high efficiency and reliable thermoelectric device the stability and high performance of TEiM/TEcM has a high contribution.

Table 0.1. Review of some thermoelectric materials

	Electrodes	Diffusion barrier	Joining Technique	Buffer layer
Bismuth telluride	Cu	Ni , V, Pt Ta-Si-N Ti-Si-N	Soldering	-
Zn_3Sb_4	Ag coated Cu	Ni	Solid liquid interdiffusion bonding	-
AgSbTe	Cu	316 stainless steel	Ag-Sn based Soldering/ Ag Nanopaste	-
PbTe	Ni,Cr,Cu,Au	SnTe, graphite foils		-
	Ni/Fe	Nb	Rapid Hot press	
	Ni/Cu	Pb foils	Hot pressing	-
$CoSb_3$	Cu, Cu-Mo, Cu-W	V, Mo, Ti,Pd,Hf,Zr,Y	Solid state synthesis	-
	Cu-Mo	Ti-Al	Solid state synthesis	-
	Mo	Ti	Solid state synthesis	-
	Ni	Mo-Ti	Solid state synthesis	Mo-Cu
$Ca_3Co_4O_9$	Ni	Fe-Cr alloy	Solid state synthesis	
	Ni	Ni+SrRuO3	Solid state synthesis	

2.2 Review of a selected thermoelectric module

2.2.1 Bonding in Bi_2Te_3 -based modules

Bismuth telluride is a semiconductor compound that has a narrow band gap, as a bulk material they are widely used in; piezo-electrics, thermostats, and refrigerators. Most of the Peltier coolers on the market are made of bismuth telluride. In thermoelectric cooling Peltier device p-type (Bi, Sb) $_2Te_3$ and n-type $Bi_2(Te, Se)_3$ are two significant semiconductors, copper (Cu) and eutectic $Sn_{42}Bi_{58}$ alloy are usually used as metallic electrode and solders respectively. Cu is chosen because it has high thermal conductivity and low electrical resistivity, but Cu exhibits donor activity in bismuth telluride and is known for its high diffusivity in bismuth telluride and formation of Cu_2Te. While the materials chosen for TEGs depends on the temperature range of operation, the device cannot survive high operating temperature since the solders and the electrode materials can diffuse into the thermoelectric material and degrade the device performance. Because of this problem, TE coolers for high temperature operating are still not available. For example, Cu can diffuse very rapidly into Bi_2Te_3 and change the carrier concentration of the material, Sn can also diffuse and reduce the thermoelectric power, so to solve this problem, a nickel (Ni) layer is used as the diffusion barrier in commercial Peltier devices.it is reported that Ni diffusion barrier layer can block

the diffusion of $Sn_{42}Bi_{58}$ solder, however, the barrier material Ni itself diffuses into Bi_2Te_3 material.

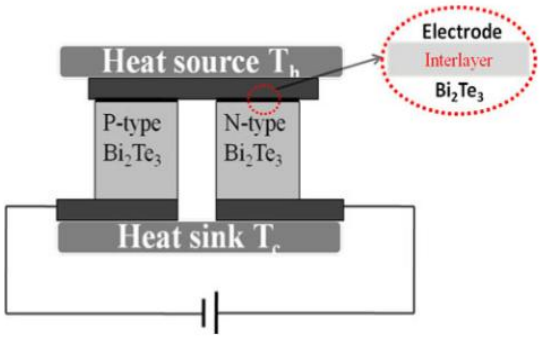

Figure 0.1. Thermoelectric modules (Electrode, interlayer, and Bi_2Te_3 based thermoelectric leg)

Additionally, several groups had studied the diffusion barrier layer for Bi_2Te_3 and Cu interconnect and reported a few of them with an encouraging result. Y.C Lan et al [89]used Ni as a diffusion-barrier layer and,the nickel diffuses into the $Bi_2(Te, Se)_3$ during the soldering processing and degrades its performance. O.D. Lyore et al[102], [103] also reported that diffusion of Ni into $Bi_2(Te, Se)_3$, produce a nickel telluride interfacial region which is mechanically weak; this result imply that nickel is not suitable as a barrier layer at the hot side in TEM, developing a new diffusion barrier layer is needed for bismuth telluride based device used for power generation. Lin et al examined silver (Ag), nickel /gold (Ni/Au), Palladium (Pd)and titanium/gold (Ti/Au) as diffusion barrier layers, reporting that titanium/gold formed the best diffusion barrier for bismuth telluride among the other based on scanning electron microscopy (SEM)results. Wen P. Lin, Pin J. Wang, et .al investigated bonding/barrier composites on Bi_2Te_3 for high-temperature thermoelectric applications. Pd, Ni, Ni/Au, Ag, and Ti/Au.

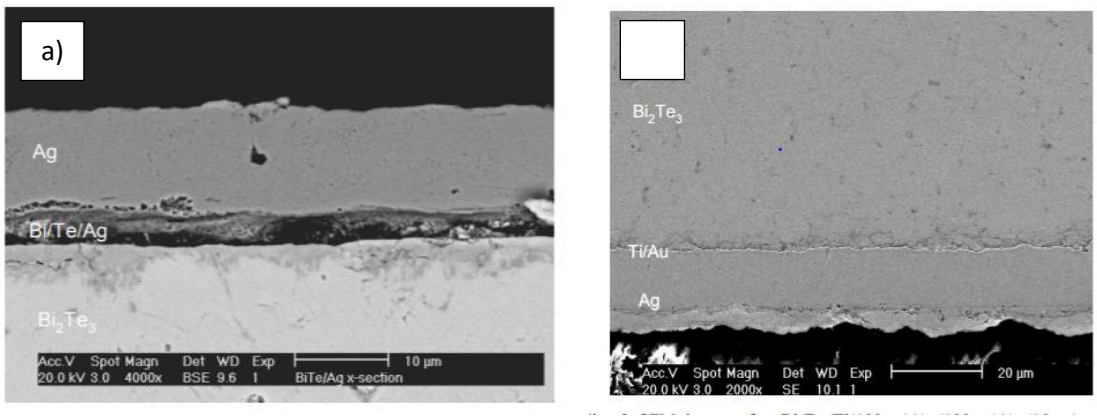

Figure 0.2. a)cross sectional SEM image of Bi_2Te_3/Ag after annealing at 250^{o}c for 10 hours, b, SEM image of a Bi_2Te_3/Ti(100nm)/Au(100nm)/Ag(10µm) sample annealed at 250℃ for 10 hours.

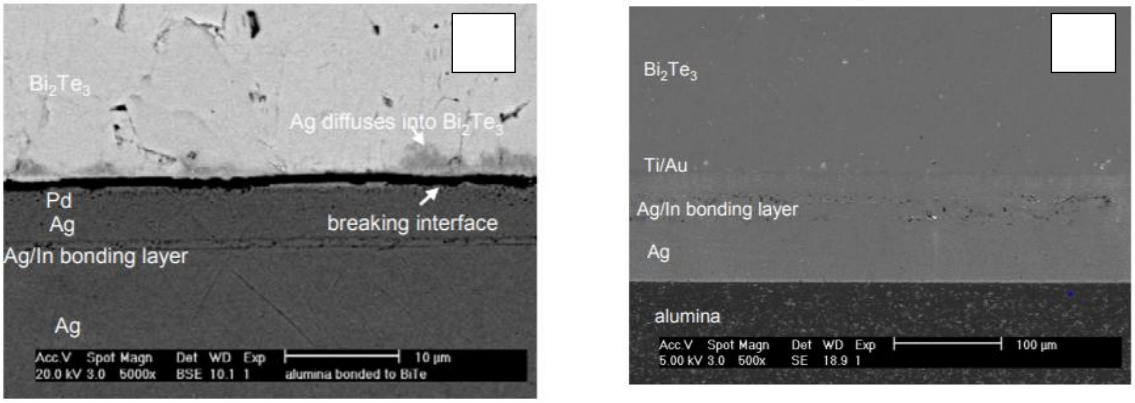

Figure 0.3. a) Cross-section SEM image of a Bi_2Te_3 a chip bonded to alumina substrate using flux less Ag-In design with Pd on a Bi_2Te_3 as the barrier layer and b) Cross-section SEM image of Bi_2Te_3 chip bonded to alumina substrate using flux less Ag-In design with Ti/Au barrier layers

The cross-section SEM image of a sample annealed for 10 hours demonstration no inter-diffusion between Ti and Bi_2Te_3 is observed. They conclude that the Ti layer bonds well to Bi_2Te_3 and Ti/Au show to be a feasible barrier for flux less bonding of Bi_2Te_3 to alumina carriers. The diffusion barrier still needs more investigation because the interlayer has an important impact on the mechanical, thermal, and electrical properties and also on the reliability of thermoelectric modules.

2.2.2 $CoSb_3$ skutterudite based thermoelectric

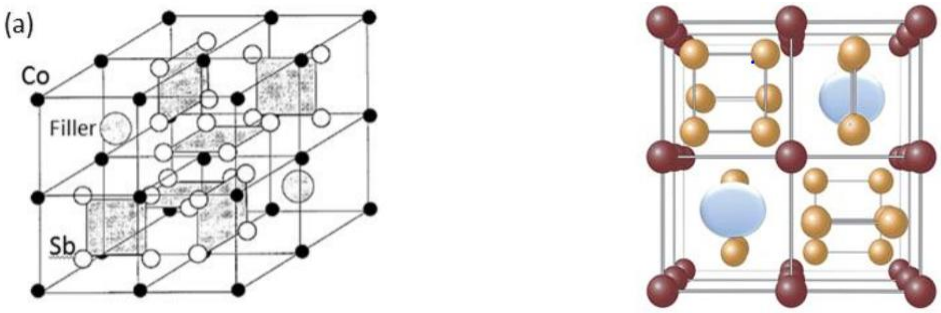

Figure 0.4. The unit cell of $CoSb_3$, the Co atoms are represented by red spheres and Sb by yellow spheres and the void cages by light blue spheres[104].

The $CoSb_3$ compound has a cage structure with two large icosahedral voids and a small band gap. $CoSb_3$- based alloys or doped $CoSb_3$ skutterudite are among the promising categories for the development of efficient thermoelectric materials. Thermoelectric efficiency related to thermal and phase stability. $CoSb_3$ based skutterudite contains volatile elements (Sb, Sr, Yb, etc) which can evaporate at operation condition, This evaporation condition may lead to structural changes and also can destroy the thermoelectric properties. The Ag-Cu eutectic alloy was used as a good braze candidate for thermoelectric modules in mid-temperature

however, Ag-Cu alloys react with the $CoSb_3$ therefore, the introduction of a barrier layer is so important and Ni, Ti, and Co are potential barrier layers.lack of excessive interfacial reaction and good wetting is important properties in joining materials, in avoiding interfacial reaction with thermoelectric substrates barrier layers or diffusion barriers play a hospital role.

2.2.3 Bonding in PbTe – based modules

PbTe -based thermoelectric materials are good aspirants for harvesting waste heat at mid-range temperatures due to both p-type[105], [47] and n -type[106] [107] high thermoelectric efficiencies. Integration of PbTe in TE devices has a significant impact on the conversion efficiency and reliability of TE device[108].a stable electrode/PbTe joints is crucial in PbTe based thermoelectric module therefore to obtain high-quality joints, several requirements must be met, one is the electrodes should not contain elements that may deteriorate TE performance. If the electrodes, solders or brazes consists of elements which will degrade the properties of TE materials or if the interdiffusion between TE materials and electrodes is rapid it is necessary to place a diffusion barrier between the electrode and TE element[109], [110]. And for good contact between diffusion barrier and the thermoelectric element the following conditions must be met; the joints should block the diffusion of the elements which may degrade the properties of thermoelectric elements, the joints should be metallurgically bonded and mechanically stable with no crack or other defects and the electrical and thermal contact resistances of the joints are required to below. To maintain a reliable and lasting mechanical bond and to meet the expectation of thermoelectric module comparable coefficients of thermal expansion (CTE) is essential for the thermoelectric material. PbTe is known for its high CTE, 20 x 10^{-6}/K, which is much higher than the refractory metals commonly used as diffusion barriers or electrodes. when compared to the metal's Ni (CTE = 13.4 x 10^{-6}/K) and Fe (CTE=11,8 x10^{-6}/K) are commonly used as diffusion barrier[111]. Compared with Fe, Ni is easier to bond to be. NiFeMo, Ag, and Nb are also some of the diffusion barriers that are investigated for PbTe TE leg and, Hot-pressing or SPS (spark plasma sintering) are major bonding methods to fabricate the PbTe- based TE modules[112], [113].

2.2.4 PbTe joints

Haiyang Xia. et.al[114]–[116] have done studies on developing PbTe based thermoelectric module. In their study, Fe, Mo, and NiFeMo alloy foils were bonded to n-type PbTe by hot pressing technique at 600, 700, and 800^{o}c under 40mpa at different holding times. They have

also done a study on Ni/PbTe joints which showed that Ni bonds well to the PbTe but reacts quickly with PbTe.

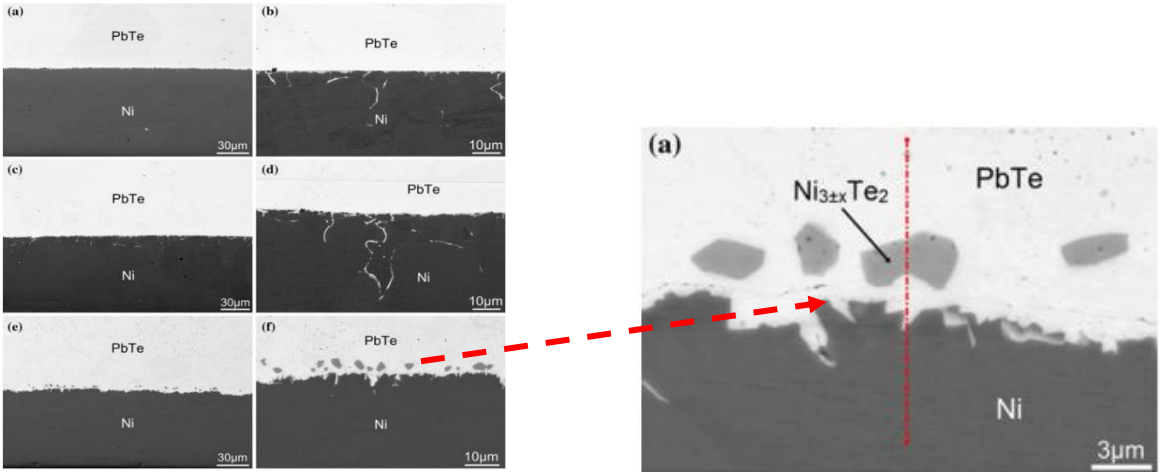

Figure 0.5. SEM micrographs of the interface of Ni/PbTe joints bonded at 600 °C for (a & b) 60 min, (c& d) 120 min and (e &f) 300 min[115].

$(3 \pm x)\ Ni(s) + 2PbTe(s) \rightarrow Ni_{3\pm x}\ Te_2(s) + 2Pb(l)$ ……..(2.3)

Increasing holding time results into diffusion of PbTe occurs, consequently binary phase β_2 precipitates as per the reaction above.

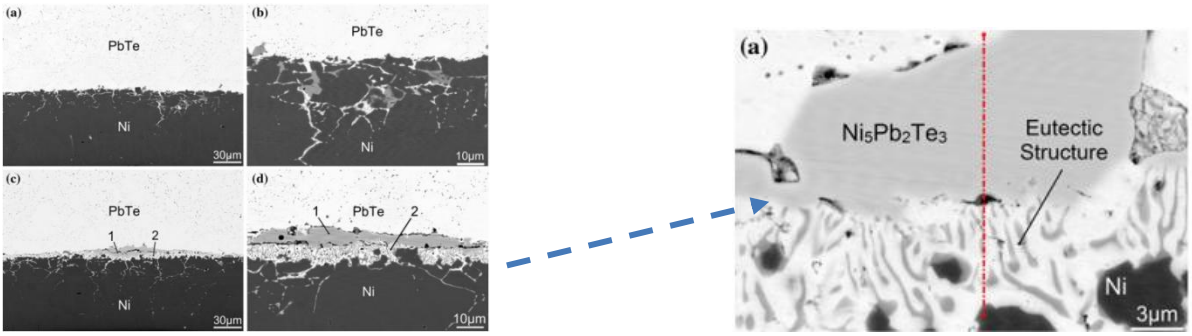

Figure 0.6. SEM micrographs of the interface of Ni/PbTe joints bonded at 650 °C for 120 min at various positions[115]

$L \longrightarrow Ni_5Pb_2Te_3 + L_{eu}$ …… (2.4)

The formation process for this microstructure can be explained by the following steps: (1) Ni atoms diffused into PbTe to form a liquid layer composed of Pb Te, and Ni at the Ni/PbTe interface during sintering (2) As the temperature was reduced, large $Ni_5Pb_2Te_3$ particle formed from the liquid layer, as described by the above reaction. (3) When the temperature eventually reached the eutectic temperature, the eutectic structure formed. X.R. Ferreres et

al.[117]. Performed one-step sintering of nickel electrode on-type PbTe powder using spark plasma sintering . The created interphase is composed of nickel telluride, which is continuous and homogeneous across the junction, without visible flaws on the electrode or in the interphase and PbTe. To assess the long-term thermal stability of the fabricated bond, an aging test was conducted at 823 K for 360 h under vacuum and Degradation of PbTe was observed after aging. The β_2 phase $Ni_{3\pm x}Te_2$was identified as the only compound formed at the Ni/PbTe interface. A uniform interphase layer of $Ni_3Te_2$with a continuous thickness of ~30μm was achieved at 793 K within 10 min. No defects were observed on the Ni electrode, allowing the reaction to occur in the contact area between the nickel and the lead telluride.

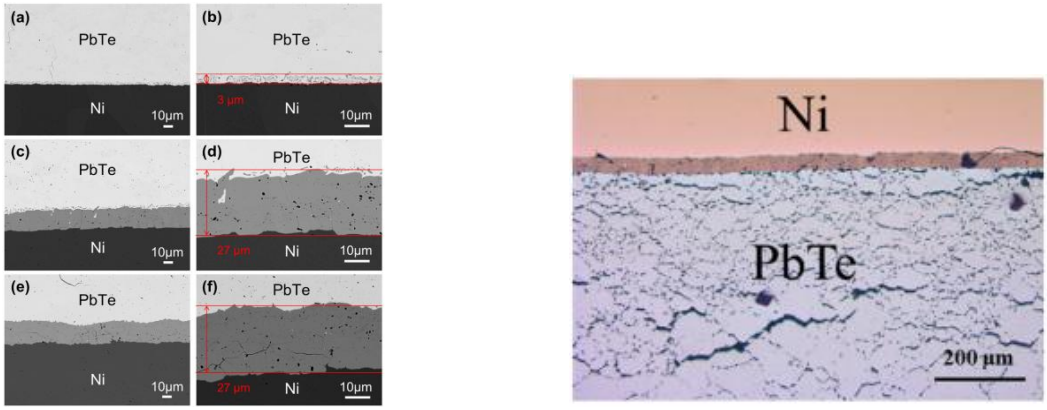

Figure 0.7. SEM micrographs of the bonding area between PbTe and Ni after sintering for 10 min at temperatures of (a) and (b) 723 K; (c) and (d) 793 K; (e) and (f)873 K. Optical microscope image after the sample was encapsulated in a quartz tube under vacuum and aged for 360 h at 823 K[117].

H Xia, CL Chen et.al. [56] Studied Interfacial Reaction between Nb Foil and n-Type PbTe thermoelectric materials they have used rapid hot-press at 700^{o}C for 60 min at a pressure of 40 MPa. A reaction layer of Nb_3Te_4 mixed with Pb was identified at the interface of Nb/ PbTe joints. Nb doesn't affect the TE properties of n-type PbTe, advantages of choosing Nb is that; Formation of a reaction layer result in metallurgical and high-strength bonding, Lower bonding temperature when compared with Fe (Hot-press at 700 °C), Low growth rate of the reaction layer, no grain boundary diffusion when compared with Ni and Reaction layer is stable till higher temperature compared with Ni, hence can withstand higher operating temperatures

The study of the growth kinetics of the Nb_3Te_4 layer discovered that the time exponent of the growth kinetics of the Nb_3Te_4 layer is about 0.61, demonstrating that the growth rate of the Nb_3Te_4 layer is controlled by diffusion as the thickness of the reaction layer increases with increasing holding time. They have explained that Nb/ PbTe joint fracture at the interface between Nb and Nb_3Te_4 and within the PbTe matrix, indicating that the bonding between Nb

and Nb_3Te_4 is weak. Mismatch of CTE (lower CTE 7.3 x 10^{-6}/K) compared with PbTe is very high. Therefore, a possible solution is the introduction of

a buffer layers.

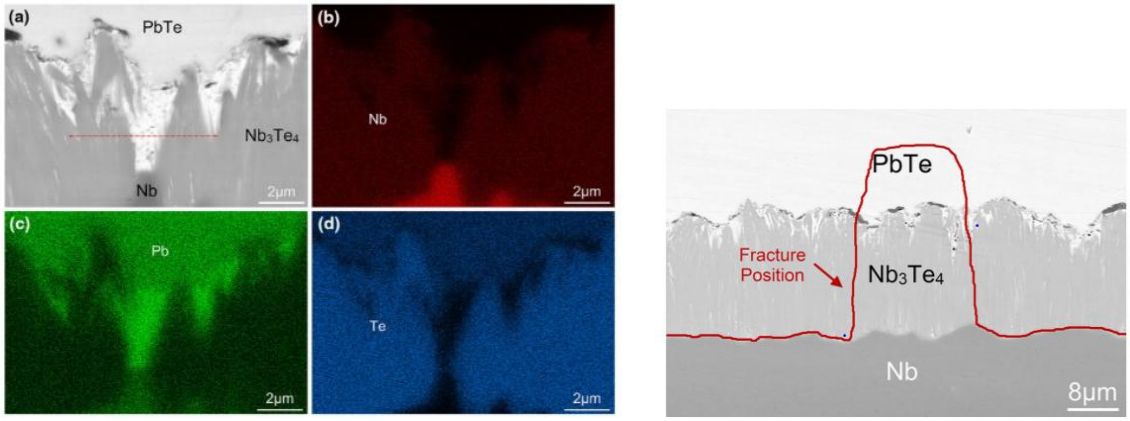

Figure 0.8. SEM micrographs of the interface of Nb/PbTe joints bonded at 700 °C for (a, b) 60 min, (c, d) 150 min, and (e, f) 300 min. 2 SEM micrograph and EDS mapping images of the interface of Nb/PbTe joints bonded at 700°C for 60 min: (a) SEM micrograph, (b) Nb element mapping, (c) Pb element mapping, and (d) Te element mapping. 3, Schematic of the fracture position of the Nb/PbTe joint bonded at 700C for 300 min[108]

Chapter Three

3. Materials and method

3.1 Materials synthesis

In this study, four-steps of material synthesis have been performed. These are:

1. Preparing thermoelectric leg (TE element) PbTe disc,
2. Preparing contact material Ni-Fe alloy disc
3. Making thermoelectric couple (PbTe/Ni-Fe).
4. Cutting, mounting and polishing

The following chart illustrates the preparation of the thermoelectric leg (TE element) PbTe disc and contact material Ni-Fe alloy disc

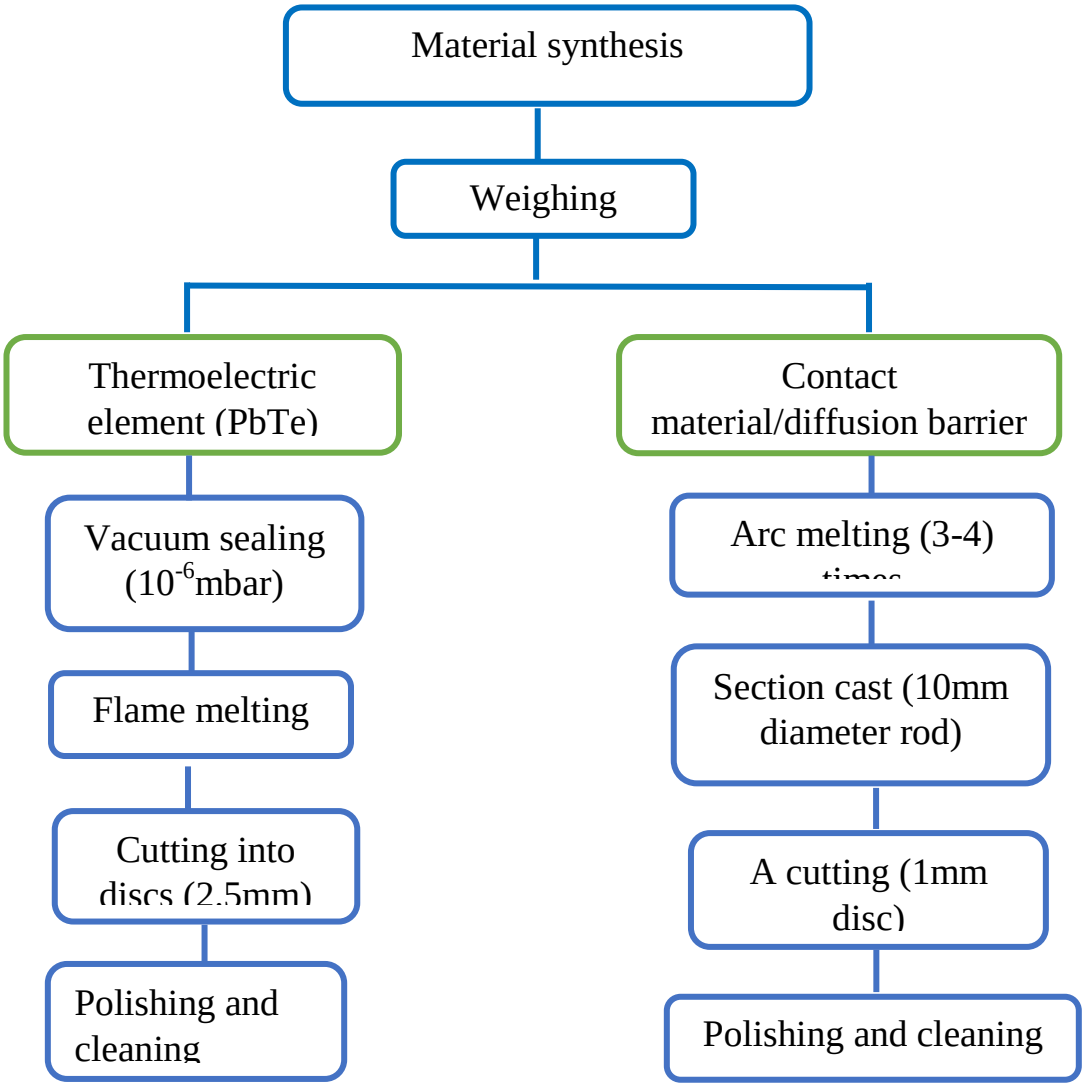

Table0.1. Atomic weight percentages of elements used

At%	Pb(wt%)	Te(wt%)	Ni(wt%)	Fe(wt%)
5%	**-**	**-**	**19.046**	**0.952**
2%	**-**	**-**	**19.618**	**0.38**
1%	**-**	**-**	**19.80**	**0.19**
50%	**12.37**	**7.62**	**-**	**-**

- Thermoelectric element (PbTe) is Vacuum sealing(10^{-6}mbar) and flame melted
- While for our Contact material/diffusion barrier (Ni-Fe alloy) we have applied Arc melting (3-4) times. Rest will be explained below.

The following chart illustrates the thermoelectric couple preparation of (PbTe/Ni-Fe).

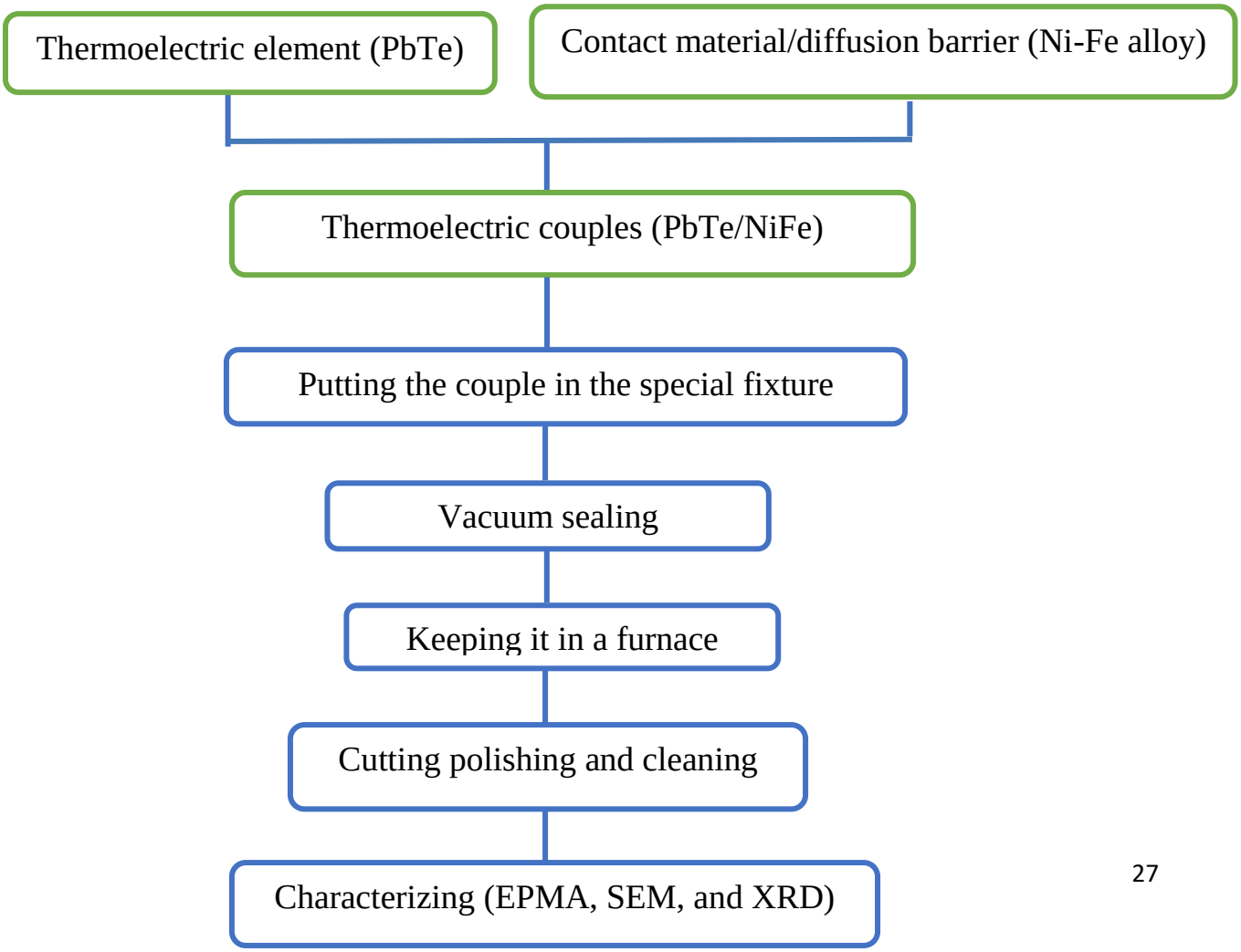

The details of the experimental procedure is as follows: To prepare the Stoichiometric PbTe thermoelectric element rod, a mixture of Pb (99.9%) and Te (99.9%) were vacuum sealed(10^{-6}mbar) in a quartz tube and flame melted until it is homogenized, followed by quenching. The resulting PbTe ingot was cut into discs (2.5mm) then polished until 4000 emery paper using a special holder to ensure the flatness of the disc and cleaned with ethanol in an ultrasonic bath. The next step is to make a contact material Ni-Fe alloy. we have taken 1%Fe,2%Fe and 5% of Fe separately to make the alloy then vacuum arc melted in Ti getting atmosphere 3 to 4 times to guarantee complete homogeneity. The Ni-Fe ingot was then suction cast into a 10mm diameter rod. The rod was then cut into discs (1mm thick) then, polished and cleaned. The third and final step is to ensure the flatness of the disc. To make diffusion bonding, this process works on the basic principle of diffusion. Diffusion means the movement of atoms under chemical potential. This is the fundamental principle of diffusion bonding. In this process, both the PbTe and Ni-Fe plates are kept in contact with each other using a special fixture with minimal pressure. This setup is kept at different temperatures for various periods which lets diffusion takes place to form various reaction products and helps to throw light on phase equilibria between materials. This diffusion can be accelerated by the application of high temperatures. the whole process takes place in a vacuum or in an inert environment that protects the plates from oxidation. the two polished discs were put in contact with each other using a special fixture. TiO_2 layer was deposited on the fixture to avoid chemical reaction between polished discs and the fixture. These were put in quartz tube and vacuum sealed (10^{-6}mbar) because sublimation for the PbTe rate is high above 500^oC. The samples were furnace cooled as well as quenched. Diffusion bonded samples were first mounted using special acrylic resin then subsequently cut in a slow-speed diamond blade cutter. Cut samples were polished on emery paper from 1500, 2000, 2500 3000, 4000-grade papers. Cloth polishing was done using a 0.3-micron Al_2O_3 suspended solution. Final polishing was done using a SiO_2 silica colloidal solution. Cloth polished sample was kept in soap water overnight and reins the soap by clean water finally the joined sample is sonicated for 20min in ethanol for further cleaning. The cleaned PbTe/Ni-Fe interface was characterized by scanning electron microscope (SEM), electron probe microanalysis (EPMA), and x-ray diffraction (XRD) technique.

In this study, the experimental analysis is done at four different temperatures (600^oc, 650^oc, 675^oc, and 700^oc) for different time intervals.

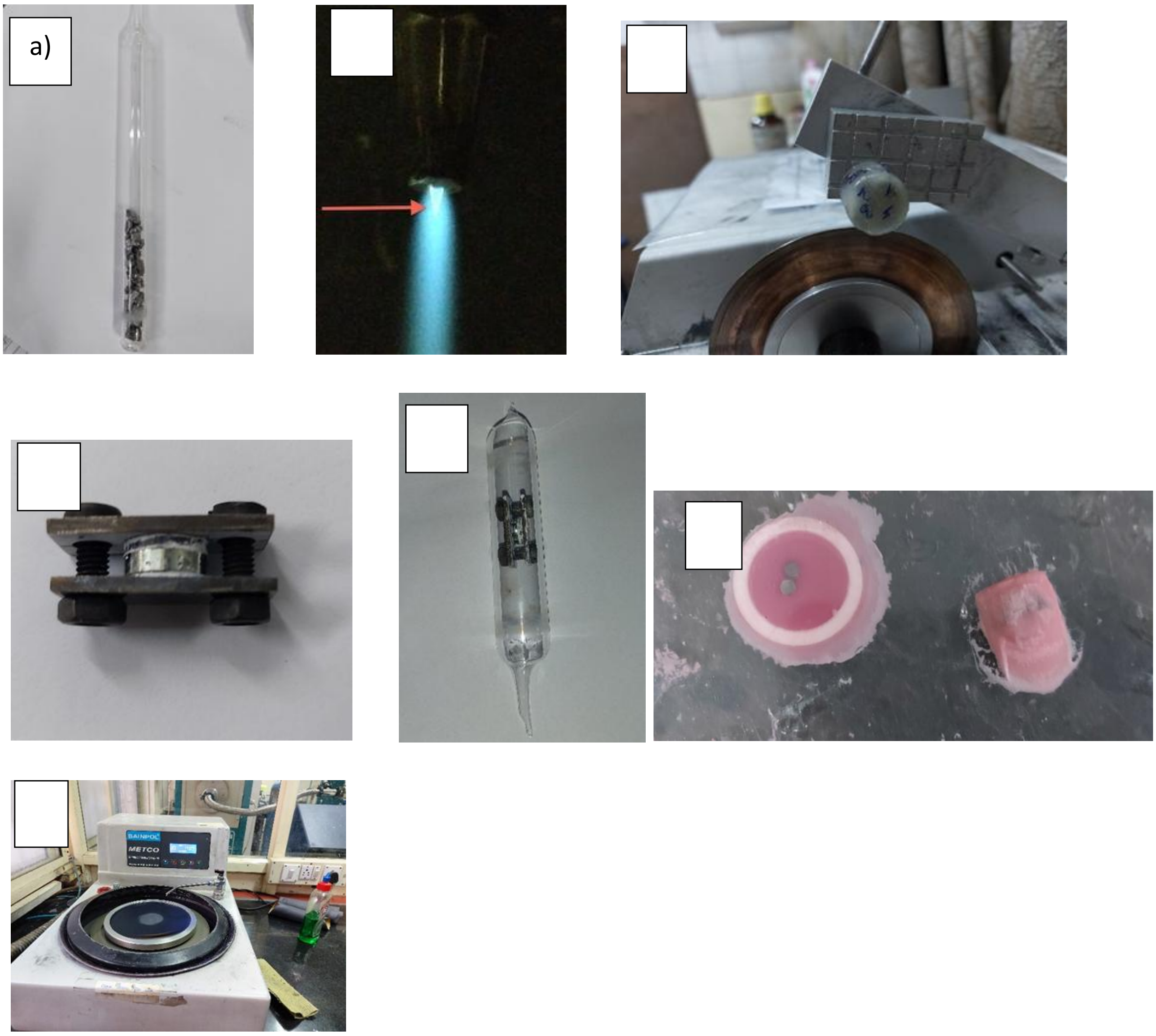

Figure 0.1. Images showing a) Vacuum sealed (PbTe), b) Flame melting, c) cutting d) PbTe/Ni-Fe couple, e) sealed PbTe/Ni-Fe couple, f) Mounted using special acrylic resin, and g) polishing

Sublimation of PbTe

At high temperature PbTe sublimates and there might be a change in stoichiometry due to the loss of the elements, consequently which may affect the thermoelectric properties of the material. Following efforts to minimize the sublimate were stated. Field and Bunde forecast that the rate of sublimation of PbTe follows the below :[118]

$$\Gamma=2\pi r_o \Upsilon T^{1/2} P \eta e^{-Ea/RoT}, \quad \text{(3.2)}$$

Where,

Γ is the rate of sublimation (kg m^{-2} s^{-1})

r_0 is the radius of the specimen

γ is the proportionality constant

T is the absolute temperature

P is the surrounding gas pressure (N m^{-2})

E_a is the activation sublimation energy (J kg^{-1})

R_0 is the universal gas constant = 24.81 J kg^{-1} K^{-1}

And η=1 for argon.

They calculated the rate of sublimation based on a fixed sample radius of 0.318×10^{-2} m. For n-type PbTe, the calculated rate of sublimation at 873 K was 2.1×10^{-7} kg m^{-2} s^{-1} at 1.722×10^{5} N m^{-2}. This rate ranged from 9×10^{-8} kg m^{-2} s^{-1} at 673 K to 6×10^{-4} kg m^{-2} s^{-1} at 873 K in vacuum. For p-type PbTe, the rate of sublimation changed from 1.9×10^{-6} kg m^{-2} s^{-1} at 723 K to 7×10^{-3} kg m^{-2} s^{-1} at 873 K in vacuum. Recent studies reported that by using positive cover gas pressure of inert argon gas a further reduction in the rate of sublimation could be achieved. In this study the PbTe were put in quartz tube and vacuum sealed (10^{-6}mbar) because sublimation for the PbTe rate is high above 500^{o}C.

3.2 Materials characterization

3.2.1 X-ray powder diffraction (XRD)

X-ray power diffraction (XRD) is a non-destructive technique primarily used for the identification of phase in a crystalline material[23]. It also gives information about the crystallographic structure, the lattice constant, unit cell dimension, the density of the material, etc. the cathode ray tube produces monochromatic radiation and its directed towards the sample, the interaction of the monochromatic ray with the crystalline sample produce constructive interference [5], [6]. when the sample and detector have rotated the intensity of the reflected x-ray is recorded. This is only possible when the wavelength of the incident x-ray beam is comparable to the interplanar distance of the crystalline phase being studied. When conditions satisfy the Braggs law ($n\lambda = 2d\sin\theta$) which relates the lattice spacing in crystalline and the diffraction angle to the wavelength of electromagnetic radiation, constructive interference occurs and a peak in intensity happens. X-ray detector used to count photon and intensity is determined by the number of counts in a certain amount of time.in this thesis we did XRD analysis to identify the intermetallic formation and phase identification.

3.2.2 SEM (scanning electron microscope)

SEM stands for the scanning electron microscope. There are two main types of the electron microscope and they use electrons for imaging. One is a transmission electron microscope (TEM) that detects electrons that pass through a very thin specimen and the other is a scanning electron microscope (SEM) that uses the electrons that are reflected or knocked off the near-surface region of a sample to create an image. The electron microscope was developed when the wavelength became the limiting factor in light microscopes. Electrons have much shorter wavelengths, enabling better resolution. In our research, we have used a scanning electron microscope (SEM). The main SEM component includes; computer and display to view the image, sample chamber, electron detector column down which electrons travel with electromagnetic lenses and source of electrons. The electron source generates electrons at the top of the column and accelerated down and passes through different lenses and apertures to generate a focused beam of an electron that hits the sample surface. SEM uses a highly energetic electron beam up to 30 keV to scan the surface of the specimen.

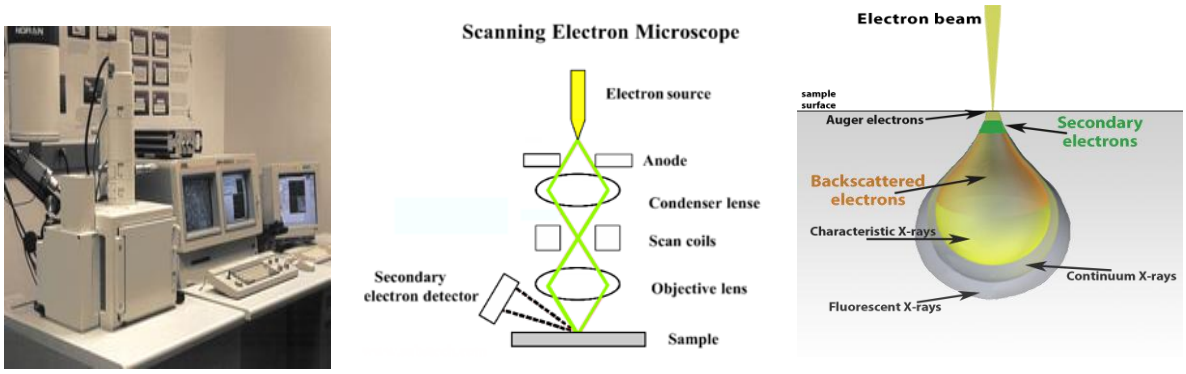

Figure 0.2. schematic representations of the basic SEM components and electron beam interaction

The interaction of electrons with a sample can generate different signals including secondary and backscattered electron, x-ray, absorbed current, and transmitted electrons. SEM uses two types of electrons for imaging, backscattered (BSE) and secondary electron (SE)[120]–[123]. BSE is reflected back after elastic interactions between the beam and the sample and SE is a result of inelastic interactions between the electron beam and sample. BSE comes from deeper regions of the sample, while SE originates from surface regions, therefore, they carry different types of information. BSE image shows high sensitivity to differences in atomic numbers. the higher the atomic number the brighter the material appears in the image. Secondary electrons are used to give the morphology (texture) and topology of sample and backscatter electrons illustrate the contrast in composition in multi-phase samples. In samples that are composed of light elements and difficult or impossible to detect in secondary

electron, the image can be an image by BSE imaging. The detector in SEM is usually an Everhart-Thornley detector that detects the secondary electrons (SE) from the near edge of the specimen. The detector amplifies the secondary electrons, converts them into a voltage, and sends them back to the signal monitor. The SEM is also capable of performing analysis of selected point locations on the sample this approach is especially useful in qualitatively determining chemical composition, crystalline structure, and crystal orientations using EDS. energy-dispersive X-ray spectroscopy (EDXS) is a supplementary unit with the SEM, which is used for quantitative chemical analysis of the specimen. EDS also used to identify and measure the abundance of elements in the sample and map their distribution. The design and function of the SEM are very similar to the EPMA.

3.2.3 Energy-dispersive X-ray spectroscopy (EDS)

Energy dispersive x-ray spectroscopy (EDS, EDX) sometimes called energy-dispersive x-ray microanalysis (EDXMA) or energy dispersive x-ray analysis (EDXA) it is an analytical technique used to analyse the elemental composition of solid surfaces and give their amount at different positions providing a map of the sample[124]. The EDS has the capability of being coupled with several applications like SEM, TEM, and scanning transmission electron microscopy (STEM). This technique relies on the interaction of some source of x-ray excitation and a sample. It follows the principle of spectroscopy, that excitation of the electronic structure of an atom can provide x-ray emission and each element has a unique set of peaks on its electromagnetic emission spectrum. The incident beam may excite an electron in an inner shell, ejecting it from the shell, while creating an electron-hole that is filled by an electron from a higher-energy shell. The difference in energy between the higher-energy shell and the lower-energy shell may be released in the form of an X-ray. The number and energy of the X-rays emitted from a specimen can be measured by an energy-dispersive spectrometer that allows us to define the elemental composition of the specimen.

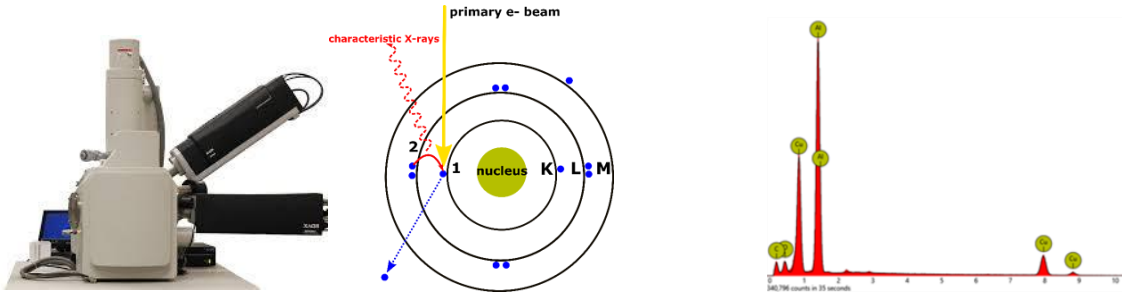

Figure 0.3. Typical EDX spectrums**.** . *The position of the peaks leads to the identification of the elements and the peak height helps in the quantification of each element's concentration in the sample.*

Analyzer, the pulse processor, x-ray detector, and the excitation source (electron beam or x-ray beam) are the EDS primary components. The detector is used to convert x-ray energy into voltage signals. And the information is sent to the pulse processor; it measures the signal and passes on to an analyser for data display and analysis. The limit of EDS is that image generation usually takes e few hours due to low x-ray intensity and it's also difficult to detect elements with low atomic numbers because the Si-Li detector protected by the beryllium window is unable to detect elements with the atomic number below 11(Na). the latest systems use the so-called silicon-drift detectors (SDDs). These are superior to the conventional Si (Li) detectors due to higher count rates, better resolution, and faster analytical capabilities. These detectors are placed under an angle, very close to the sample, and can measure the energy of the incoming photons that belong to the X-rays. The higher the solid angle between the detector and the sample, the higher the X-rays' detection probability, and therefore the likelihood of acquiring the best results.

3.2.4 EPMA (electron probe micro-analyser)

EPMA stands for an electron probe micro-analyser. it is also informally called an electron microprobe or just probe. It is fundamentally the same as an SEM but with the extra capability of analysis.it provides a much better result than standard SEM/EDS systems, because of the internal properties of WDS. The spectral resolution and detector time are much better than energy dispersive spectroscopy (EDS). EPMA is both a qualitative and quantitative method of non-destructive elemental analysis at a very small spot size (1-2microns). It works by bombarding an electron (typical energy 5-30kev) beam to the sample and collecting the x-ray photons which are emitted by various elemental species.it measures the wavelength or energies of emitted X-rays by WDX or EDX.WDS uses Bragg diffraction from to select X-ray wavelengths and, EDS uses a solid-state semiconductor detector to gather X-rays of all wavelengths produced from the sample. Chemical composition is determined by comparing the intensities of characteristic X-rays from the sample material with intensities from the known composition (standards). Variations in chemical composition within a material (zoning), such as a mineral grain or metal, can be readily determined. When the scattered electrons from the sample interact with bound electrons in the innermost electron shells of the atoms of the various elements in the sample, they can scatter the bound electrons from the electron shell creating a vacancy in that shell

(ionization of the atom). This vacancy is unstable and must be filled by an electron from either a higher energy bound shell in the atom forming another vacancy which is in turn filled by electrons from yet higher energy bound shells or by unbound electrons of low energy. The difference in binding energy between the electron shell in which the vacancy was produced and the shell from which the electron comes to fill the vacancy is emitted as a photon. The energy of the photon is in the X-ray region of the electromagnetic spectrum. As the electron structure of each element is unique, the series X-ray line energies produced by vacancies in the innermost shells is characteristic of that element.

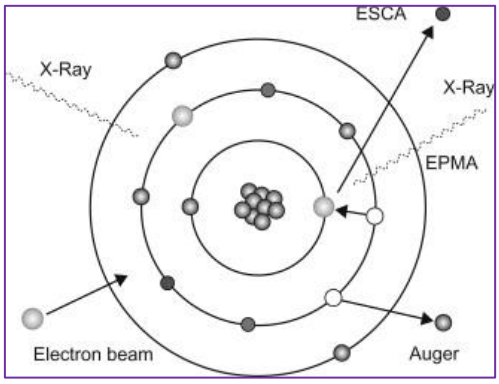

Figure 0.4. Photoelectric emission processes

EPMA involves of four main components, these are; An electron source, A sequence of electromagnetic lenses positioned in the column of the tool(used to condense and focus the electron beam coming from the source), A sample chamber, with movable sample stage (X-Y-Z), that is under a vacuum to prevent gas and vapor molecules from interfering with the electron beam on its way to the sample. and A diversity of detectors that are set around the sample chamber to collect x-rays and electrons emitted from the sample. Limitations of this EPMA instrument are that Even though electron probes can analyse for nearly all elements, WDS cannot determine elements below number 5 (boron) they are unable to detect the lightest elements (H, He, and Li). Some elements generate x-rays with overlapping peak locations (by both energy and wavelength), Probe analysis also cannot differentiate between the different valence states of Fe, so the ferric/ferrous ratio cannot be determined and must be evaluated by other techniques

Chapter Four

4. Result and discussion

4.1 Diffusion kinetics

Annealing temperature of 600 °C and time of 10 hours

The microstructural images of Ni- (1, 2, 5 at %) Fe/PbTe annealed at 600 °C for 10 hours is depicted in the following figures together with the elemental composition analysis.

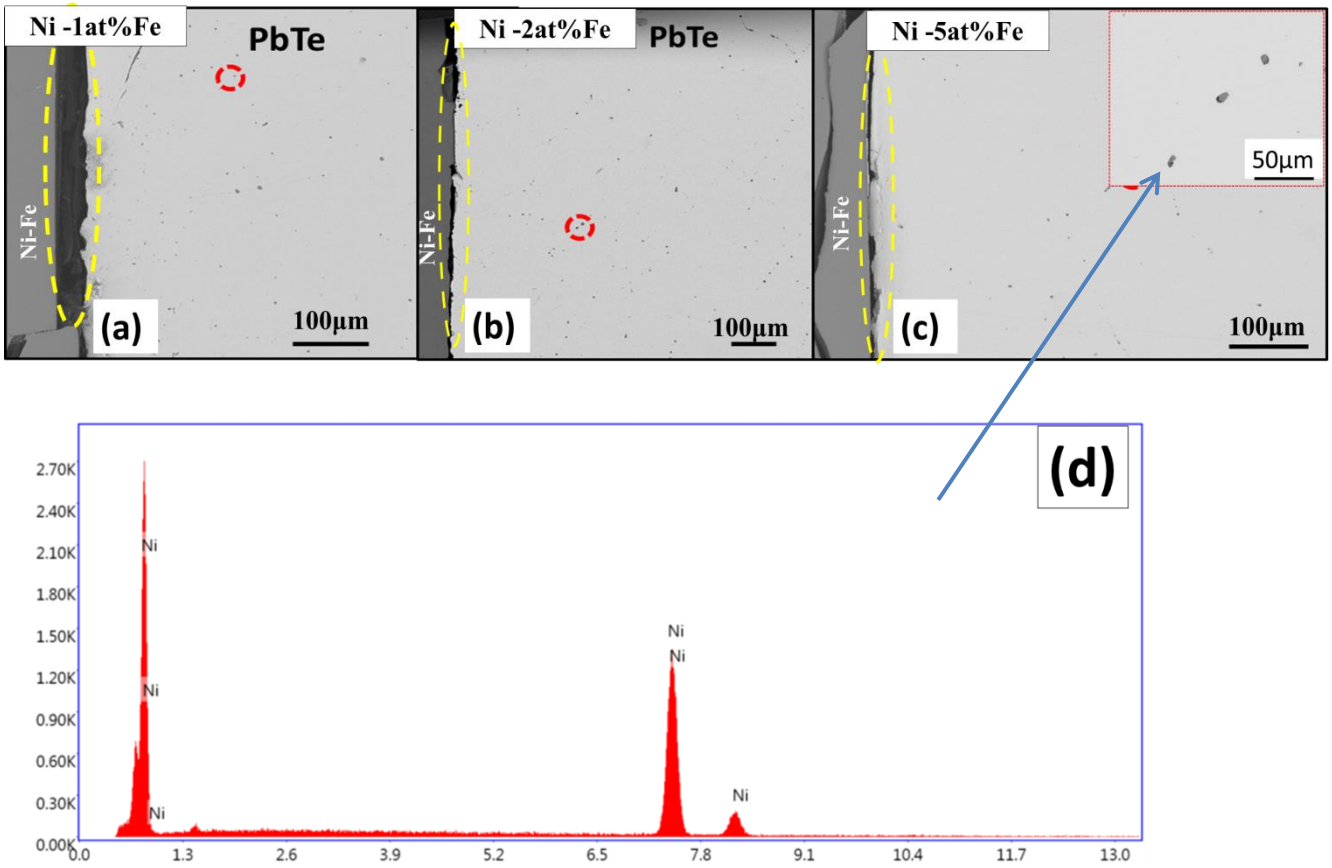

Figure 0.1. Three composition of the diffusion barrier sample (a-c) undertaken with PbTe at 600 °C for 10 hours. d) EDS elemental analysis

Figure 4.1 a) to c) shows the diffusion kinetics of Ni-Fe/PbTe microstructure with different composition of Fe at 600^{o}c for 10 hours. In figure 4.1 a) the phase with dark contrast is Ni-Fe and the phase with grey contrast is PbTe, the same also can be said for b) and c), .Backscattering image shows high sensitivity to differences in atomic number, the higher the atomic number the brighter the material appears in the image (atomic no. pb= 82, Te= 52, Ni= 28 and Fe= 26). This is further confirmed by EDS elemental analysis. while the yellow circled region is the interface, and it is detached during cutting; because of weak bonding and from the micrograph it can be concluded that the Interfacial microstructure of Ni-Fe /PbTe joints are weakly bonded at 600^{o}c holding for 10hrs. We can also observe that Ni

slightly diffuse in to PbTe side conformed by dark, Isolate red circled Ni precipitates at PbTe side. Which is further identified by fig.4.1 c) EDS elemental analysis, while no Ni-Te intermetallic were observed. The addition of Fe completely suppresses the reaction of Ni-Te.

Annealing temperature of 650 °C and time of 25 hours

The following microstructure is the result of the Ni-1 at %Fe PbTe annealed at a temperature of 650 °C for annealing time of 25 hours.

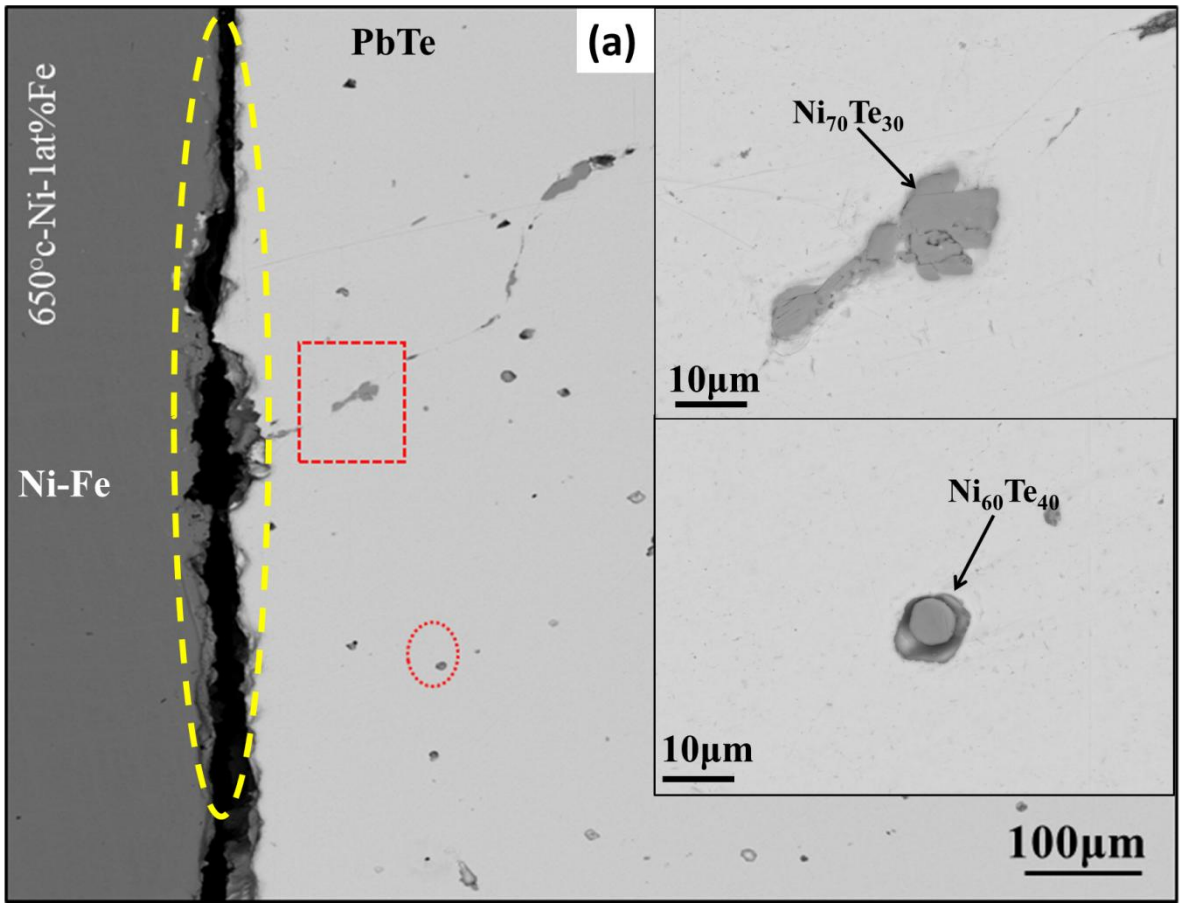

Figure 0.2. SEM micrographs of the interface of Ni-Fe/PbTe joints at 650 °C for 25 hrs-1at%. and EDS elemental analysis of the interface.

To optimize the bonding temperature we further did an experiment at 650°c for 25hours holding time shown on Fig.4.2. The phase with dark contrast is Ni-Fe and the phase with grey contrast is PbTe while the yellow circled region is the interface. Based on EDS elemental analysis Intermetallic of Ni and Te is observed with composition- $Ni_{70}Te_{30}$ and $Ni_{60}Te_{40}$ for the 25hrs holding time Ni-1at%Fe/PbTe sample shown on fig.4.2. The interface is detached (darker area at the interface) again during cutting showing that the interface is still weak. At this temperature (650°c), first $Ni_{70}Te_{30}$ phase is more favourable to form, once it precipitates out, it gradually transforms into equilibrium Ni_3Te_2; it's a kinetically driven process.

Annealing temperature of 675 °C, annealing time of 1 hours of Ni- (1, 2,5at %) Fe/PbTe

The Back scattered electron images (BSE) the samples of Ni-(1, 2,5at %) Fe/PbTe is depicted in the following figure together with the elemental composition analysis of Ni-2atFe PbTe by line scan.

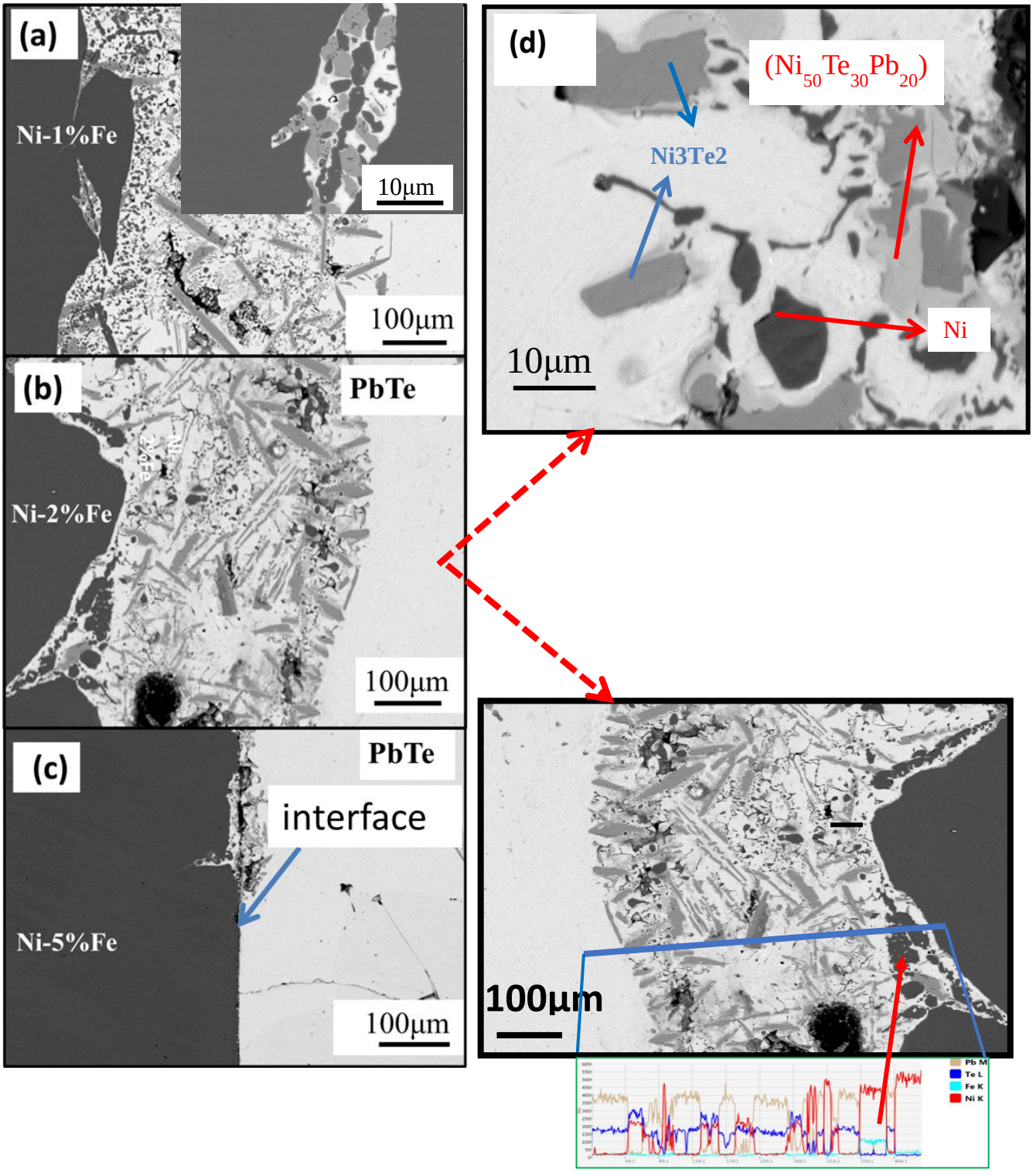

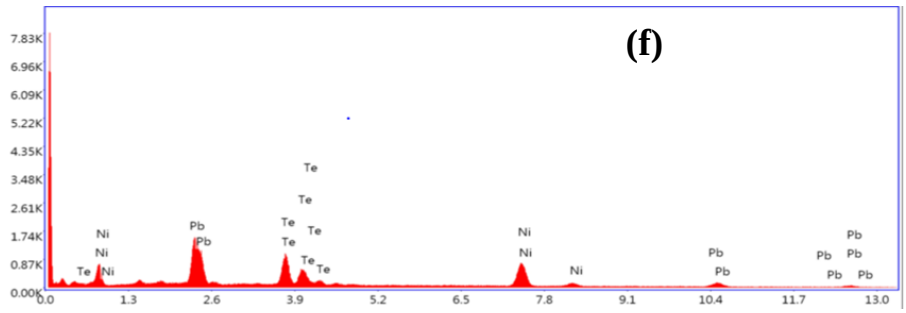

Figure 0.3. a) BSE image of Ni-1at% Fe/PbTe, b) Ni-2at %Fe/PbTe, c) Ni-5 at %Fe/PbTe, d) high magnification BSE image of Ni-2at %Fe/PbTe, e) line scan analysis of Ni-2at %Fe/PbTe, and f) the elemental analysis Ni-2at %Fe/PbTe

Table 0.1. Table showing the contrast of the elemental analysis of the Ni-2at %Fe/PbTe obtained from the above microstructural analysis

Phase	**Ni(at%)**	**Te(at%)**	**Pb(at%)**	**Fe (at%)**
White contrast	-	47±2	49±1	-
Dark contrast	87±2	-	-	9±2
Light grey contrast	48±4	28±4	20±3	-
Dark grey contrast	59±1.5	38±2	-	-

Figure 4.3 a) to d) shows the microstructure of the diffusion kinetics of Ni-Fe/PbTe with different composition of Fe at 675^{o}c for 1 hour. In figure 4.3 a), b) and c) the phase with dark contrast is Ni-Fe and the phase with grey contrast is PbTe while the interface is shown by arrow on c) is high magnification for reaction region to identify the phases. And e) shows the EDS elemental analysis done for this region reveals that different phases are present, as mentioned in the above table, these phases are PbTe, Ni-Fe, ternary phase ($Ni_{50}Te_{30}Pb_{20}$) and β_2. The 675^{o}C Ni-Te reaction is preceded by chemical reaction with formation of $Ni_{50}Te_{30}Pb_{20}$ and Ni_3Te_2 as reaction products. Isolate precipitates of Ni with enriched Fe is

also observed. Study of the growth kinetics of diffusion layer discovered that the growth rate of Ni is more in 1%Fe than 2% Fe and 5%Fe. The thickness of the reaction layer increases at the same holding time. To further identify composition of the diffusion layer, energy dispersive spectroscopy (EDS) was used for line analysis and the result is shown in fig;4.3. e) It comes with the Fe enrichment near the interface

Annealing temperature of 700 °C, annealing time of 15, 30, and 60 minutes of Ni- (1 and 5 at %) Fe/PbTe

The BSE images of the samples of Ni- (1 and 5 at %) Fe/PbTe annealed at an annealing temperature of 700 °C and annealing time of 15, 30, and 60 minutes is depicted in the following figure.

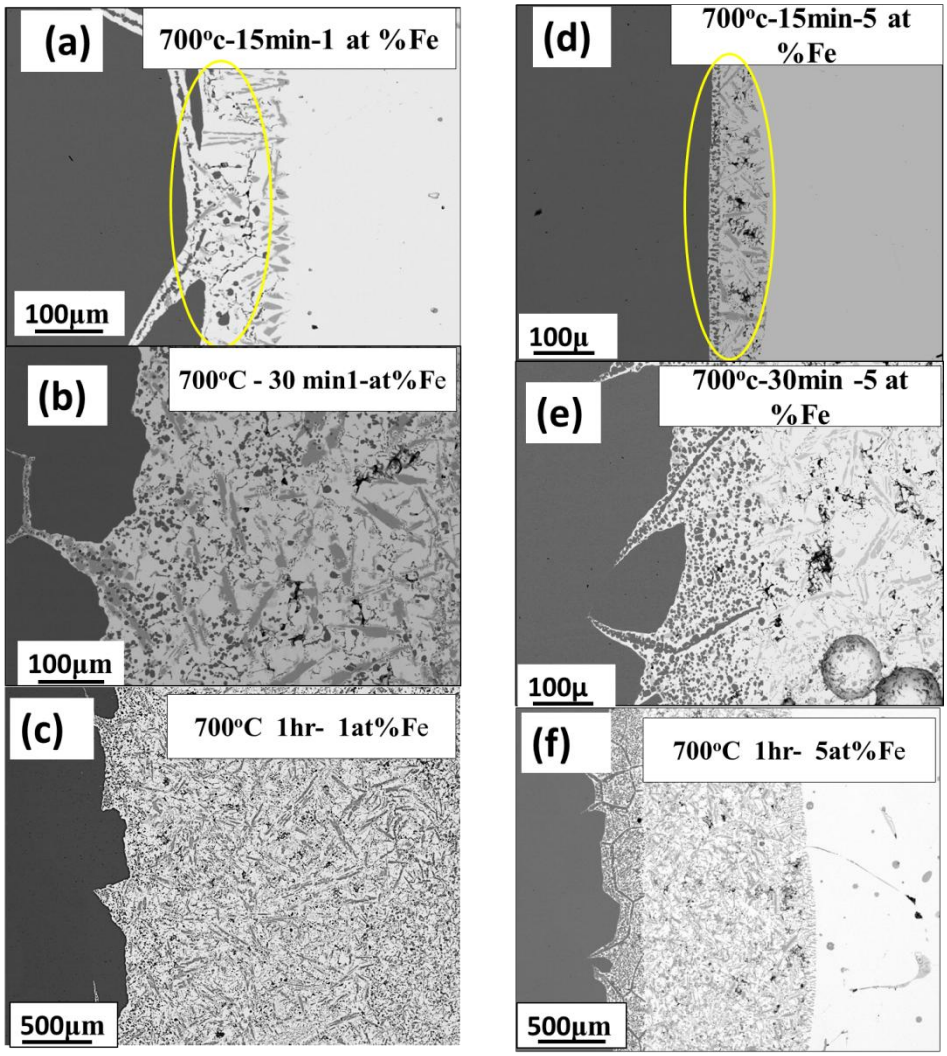

Figure 0.4. SEM micrographs of the interface of Ni-Fe/PbTe joints at 700 °C for 15min, 30min and1hr

SEM microstructure of the diffusion kinetics is show in Figure 4.4 with two composition of the Ni-Fe/ PbTe at 700 °C for 15, 30min &60min ;a) diffusion couple reaction for Ni -1at%Fe/PbTe -15min,b) diffusion couple reaction for Ni -1at%Fe/PbTe-30min ,C) diffusion couple reaction for Ni -1at%Fe/PbTe- 60min,d) diffusion couple reaction for Ni 5at%Fe/PbTe- 15min,e) diffusion couple reaction for Ni -5at%Fe/PbTe- 30min,and f) diffusion couple reaction for Ni -5at%Fe/PbTe- 60min.four phases in this samples could be easily differentiated by colour contrasts, which were identified to be Ni_3Te_2(grey), Ni(black). PbTe (white) $Ni_5Te_3Pb_2$ (light grey). Since the diffusion and formation of intermetallic compound damage the excellent property of our thermoelectric materials choice of optimum temperature and time is crucial, as stated on figure 4.4 we have also compared two different composition of the contact material to optimize the composition. Compering of 1 and 5at%Fe we can observe that the addition of Fe is slowing down the reaction rate. A sample with 1at%Fe is more reacted. Suggesting the 700^{o}c – 15min-5at%FeNi/PbTe result is with low intermetallic formation and diffusion.

XRD result of the interface (PbTe/Ni-Fe) at 700 °C

The XRD of the interface of (PbTe/Ni-Fe) at 700 °C is presented in the following figure.

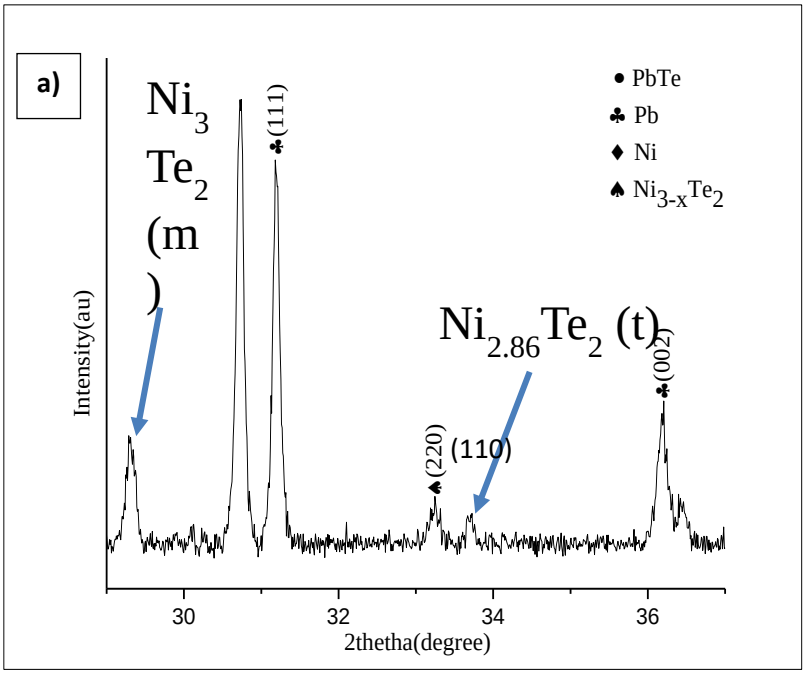

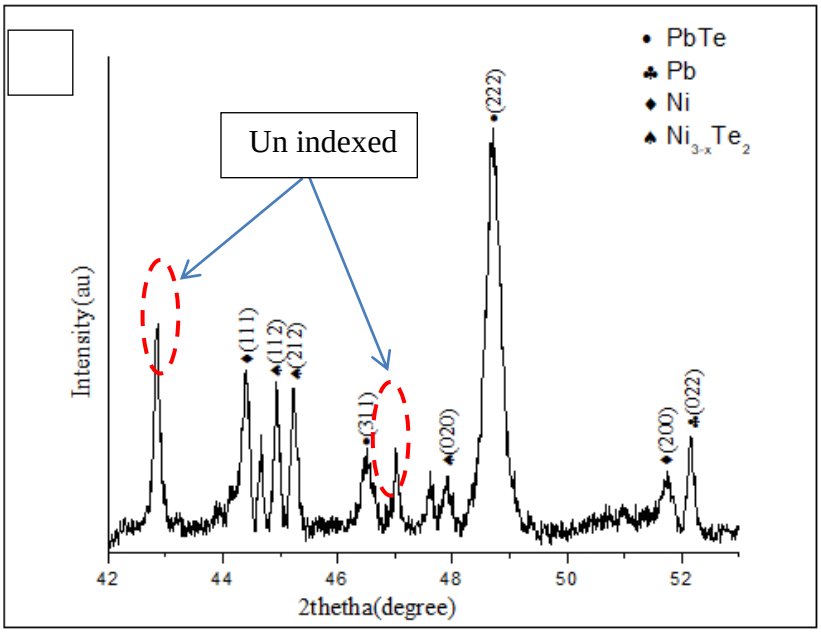

Figure 0.5. XRD result of the of the interface (PbTe/Ni-Fe) annealed at 700 °C for 60 minutes (a) in the 27 – 38 2 theta and (b) from 42 – 53 2 theta ranges.

$Ni_{3-x}Te_2$ is non-stoichiometric compound. It has different crystal structure depending on Ni concentration and temperature. Ni rich $Ni_{3-x}Te_2$ has monoclinic crystal structure at lower temperature and Ni_3Te_2 has monoclinic structure which is stable at lower temperature. $Ni_{2.86}Te_2$ has tetragonal structure, as couples were quenched from 700 °C; it retains some high temperature tetragonal phase as well. Unindexed peaks likely to be originating from ternary $Ni_5Pb_2Te_3$ phase, as we observed from EDS elemental analysis, since no crystallographic information is available, those couldn't be indexed.

β_2 ($Ni_{3\pm x}Te_2$) phase analysis

The following phase diagram further confirms the phase formed at the annealing temperature of 700 °C for an annealing time of 60 minutes

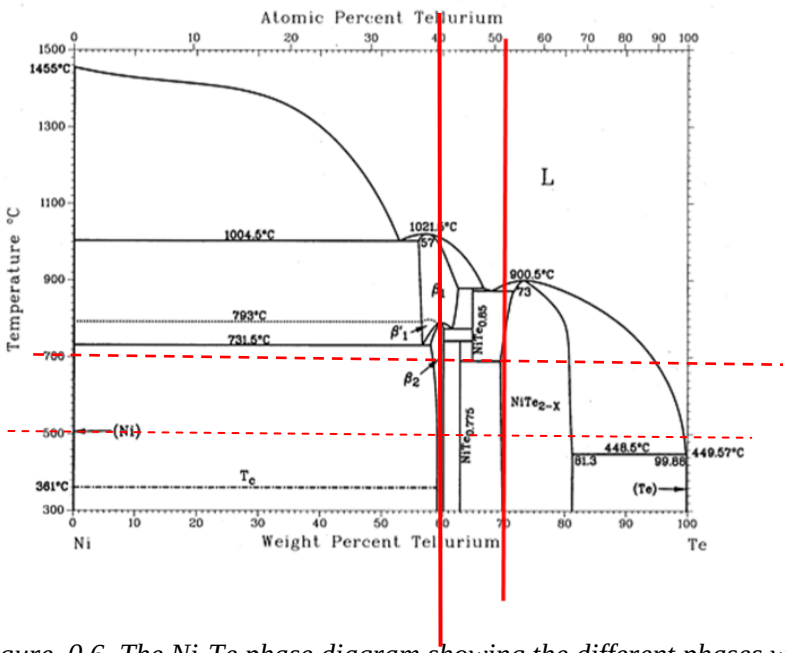

Figure 0.6. The Ni-Te phase diagram showing the different phases with respect to temperature and weight percentage of tellurium.

The Ni_3Te_2 phase formed belongs to the β_2 phase in Ni-Te system as we can see from figure 4.7. The reaction taking place at the interface between Ni and PbTe is represented in equation (4.1) as discussed Ferreres et al. [117]. Their study which contains liquid lead and solid nickel telluride as the reaction products.

$$(3\pm x)\ Ni(s) + 2PbTe(s) \rightarrow Ni_{3\pm x}Te_2(s) + Pb(l) \quad \ldots\ldots 4.1$$

Using a theoretical resistance of 3.2×10^{-3} for Ni ,Ferreres et al. [125] reported the electrical resistance for Ni_3Te_2 and interface contacts with Ni and PbTe is of 1.87mΩ.

Table 0.2. Crystallographic structures, lattice parameters, and transition temperatures of (β_2) $Ni_{3\pm x}Te_2$ phase.

(β_2)$Ni_{3\pm x}Te_2$	Transition temperature	Crystal structure	a(Å)	b(Å)	c(Å)	β(°)	Reference
Ni_3Te_2		Monoclinic	7.5382	3.7934	6.0883	91.159	[126], [127]
$Ni_{2.88}Te_2$	491 K	orthorhombic	7.5382	3.7879	6.0647	90	[126], [127]
$Ni_{2.86}Te_2$	610 K	Tetragonal	3.7820	3.7820	6.0620	90	[126], [128]

Ni- Te system is complex and it presents different crystal structures for room temperature. The recent studies tells that this disorder transition between the tetragonal- orthorhombic – monoclinic crystal structures of the (β2)$Ni_{3\pm x}Te_2$ is because when cooling to room temperature the ordering of the interstitial Ni atoms located at the octahedral sites of the monoclinic crystal takes places[129], [130]. One should know that there is no $Ni_5Te_3Pb_2$ crystallographic information reported yet.

4.3 Fe enrichment

Temperature 700 °C, 15 min, Ni- Fe (1at% & 5 at%)/ PbTe

The BSE image of the samples annealed at 700 °C, 15 min, Ni- Fe(1 at % & 5 at %)/ PbTe is depicted in the following figure.

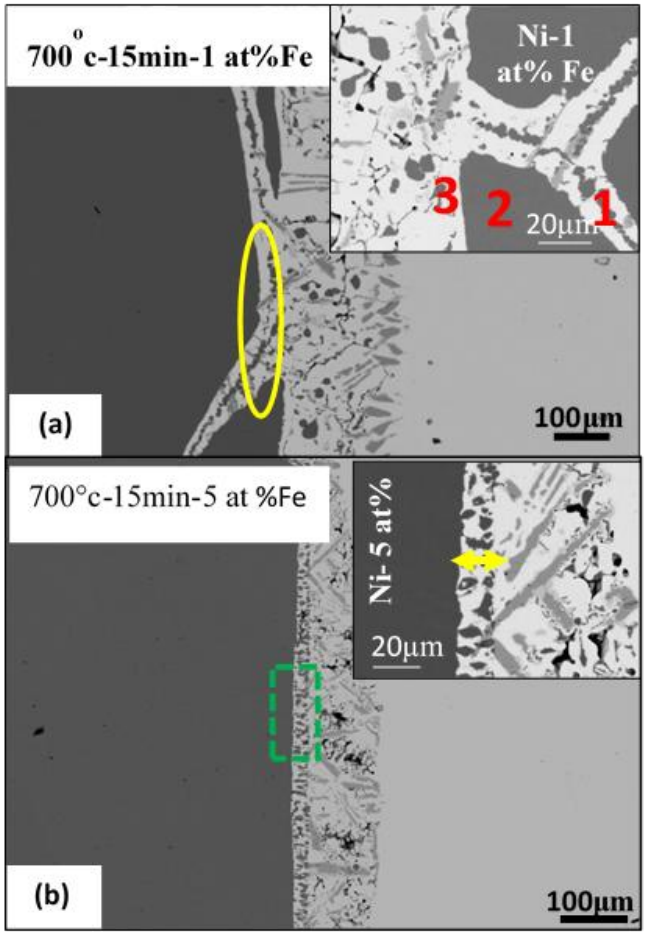

Figure 0.7. EDS elemental analysis shows enriched Fe at different places from the interface for (700°C for 15 minutes) on samples of Ni- Fe (1at% & 5at%)/ PbTe a) Diffusion couple reaction for Ni -1at %Fe/PbTe -15min-700 °C. Inset shows Fe enriched Ni precipitates at the grain boundaries in the Ni side shown by yellow circle. (b) Diffusion couple reaction for Ni -5at%Fe/PbTe -15min-700 °C and the inset shows Fe enrichment near the interface shown by yellow arrow .moreover we have also done this analysis for (700 °C -30- min) sample.

The following table presents the percnetages of Ni, Te, Pb, and Fe in the sample Ni- Fe (1at% & 5at%)/ PbTe

Table 0.3. Corresponding elemental composition analysis on the sample of Ni-1at% Fe/ PbTe on the area denoted as 1, 2, and 3 in the above microstructure.

point	Ni(at%)	Te(at%)	Pb(at %)	Fe(at %)
1	87±3	-	-	10±3
2	99±1	-	-	1±0.5
3	98±2	-	-	-

The following figure presents the microstrucre and the corresponding elemental analysis to illustrate the Fe enrichment at different regions in the microstructure.

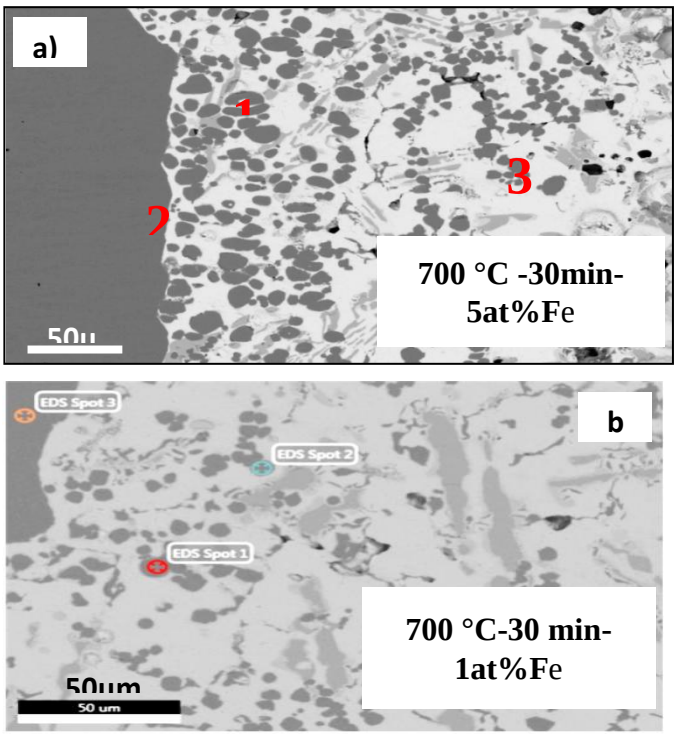

point	Ni(at%)	Fe(at%)
1	83±1	16±1
2	94±1	5±1
3	80±3	17±3

point	Ni(at%)	Fe(at%)
1	88±2	9±2
2	88±2	9±2
3	99	1

Figure 0.8. Microstructure showing the EDS elemental analysis of Fe enrichment at different places from the interface for (700 °C for 30 min)

We kept the two samples (Ni- 5 at% Fe)/PbTe and (Ni- 1 at% Fe)/PbTe in the furnace at 700^{o}C for 30 minutes and the PbTe side is almost entirely reacted but the Fe enrichment is still happening as described in Fig. 4. 7 by EDS elemental analysis result. a) Diffusion couple reaction for Ni -5at%Fe/PbTe-30min-700^{o}c, Points shows enriched Ni at different places from the interface ,(b) is for diffusion couple reaction of Ni -1at%Fe/PbTe-30min-700^{o}c .Enrichment is lesser compared to 5at% Fe as the maximum enrichment was found to be <10 at%Fe.

Ni-5at%Fe/PbTe sample annealed at 700 °C for 1 hour

The following figure is further analysis of the microstructure of Ni-5at%Fe/PbTe sample subjected to annealing of 700 °C for about 1 hour of annealing time.

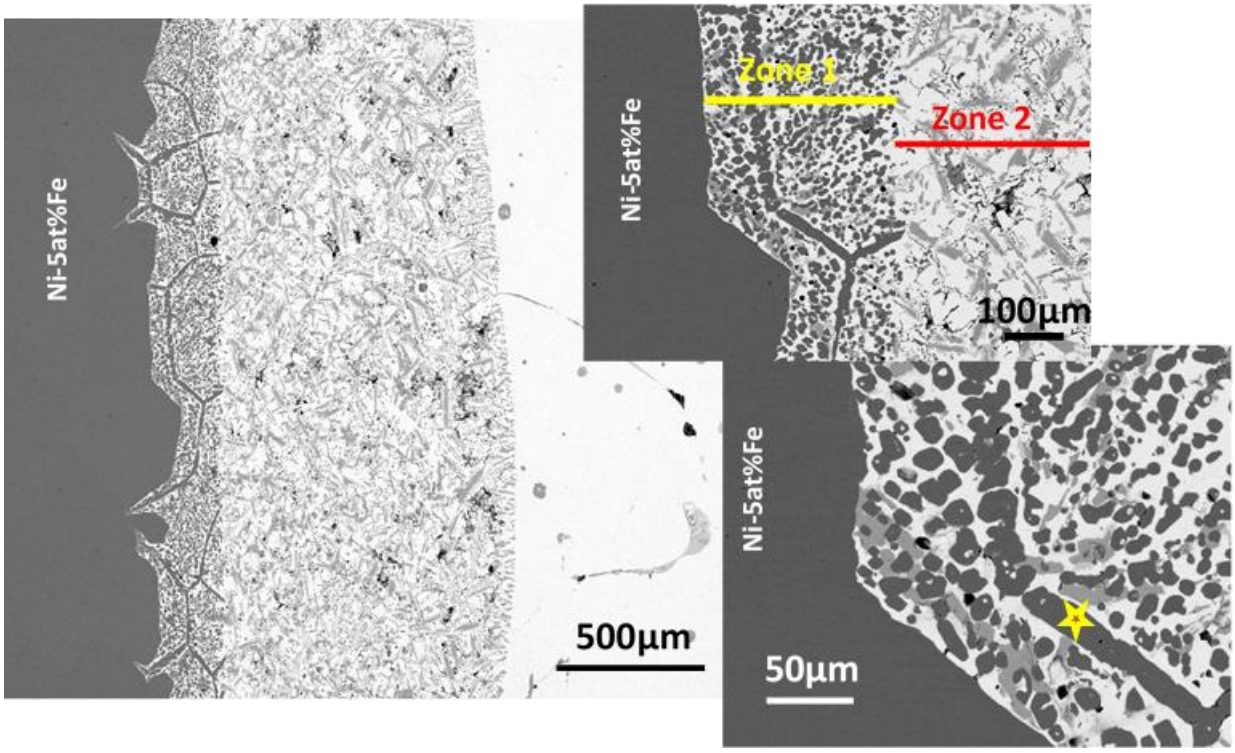

Figure 0.9. Microstructure of Ni-5at%Fe/PbTe subjected to annealing temperature of 700 C for 1 hour showing different zones of Fe enrichments.

At 700 °C, Ni-1at%Fe/PbTe joint interface Mixture of phases (Ni, β_2 (Ni_3Te_2), ($Ni_{50}Te_{30}Pb_{20}$) and Pb) were observed and the entire PbTe side is reacted. But for Ni-5at%Fe/PbTe joint interface, two distinct layers are observed fig; 5.8 **Zone 1:** Enrichment of Fe was found near the interface. Reaction products were found in the entire PbTe side, suggesting rapid reaction between diffused Ni and PbTe. Closer to interface Fe enriched Ni precipitates were found

denoted by p by star. **Zone 2:** mixture of phase is found; $\beta_2(Ni_3Te_2)$, Ni, ternary phase ($Ni_{50}Te_{30}Pb_{20}$). Zone 2 from above sample was further analysed of its composition with regard to Ni, Te, Fe and Pb, which is presented in the figure below.

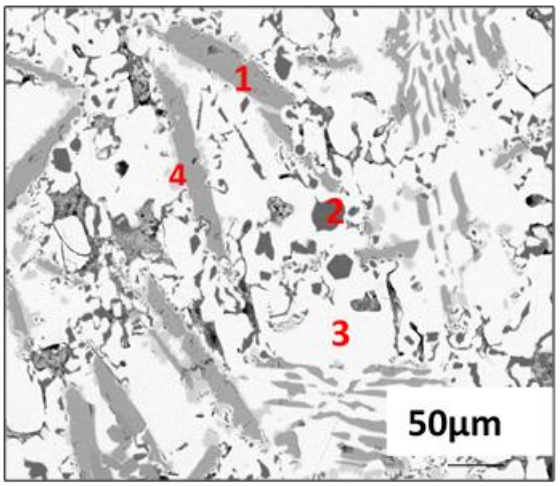

Phase contrast	Ni(at%)	Te(at%)	Fe(at%)	Pb(at%)
Grey	59±1.5	38±2	-	-
Dark	100	-	-	-
white	-	47±2	-	49±1
Light grey	48±4	28±4	-	20±3

Figure 0.10. Mixture of phase is found in the analysed zone: The phase are 1) $\beta_2(Ni_3Te_2)$, 2) Ni, 3) PbTe, and 4) ternary phase ($Ni_{50}Te_{30}Pb_{20}$)

The EDS elemental mapping was performed to observe how Fe is enriched in the grain boundaries, as reported below.

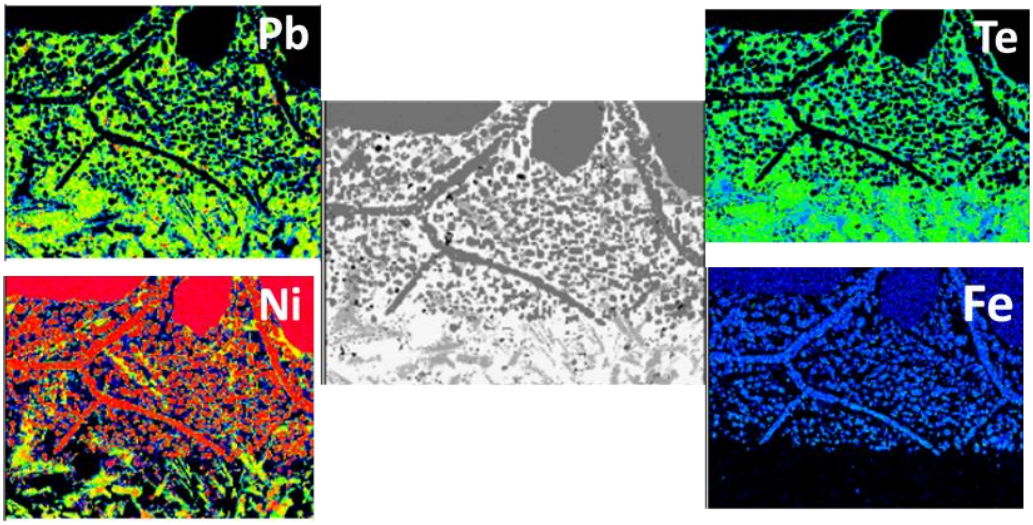

Figure 0.11. EDS elemental mapping of bonded PbTe/Ni-Fe at 700 °C for 1 hour

The following plot shows the comparison for change in thickness of reaction layer with time done for 1at%Fe-Ni/PbTe and 5at%Fe-Ni/PbTe sample at 700 °C. The result shows that with time, reaction will increase and the overall reaction zone is high for the 1at%Fe-Ni/PbTe than 5at%Fe-Ni/PbTe sample.

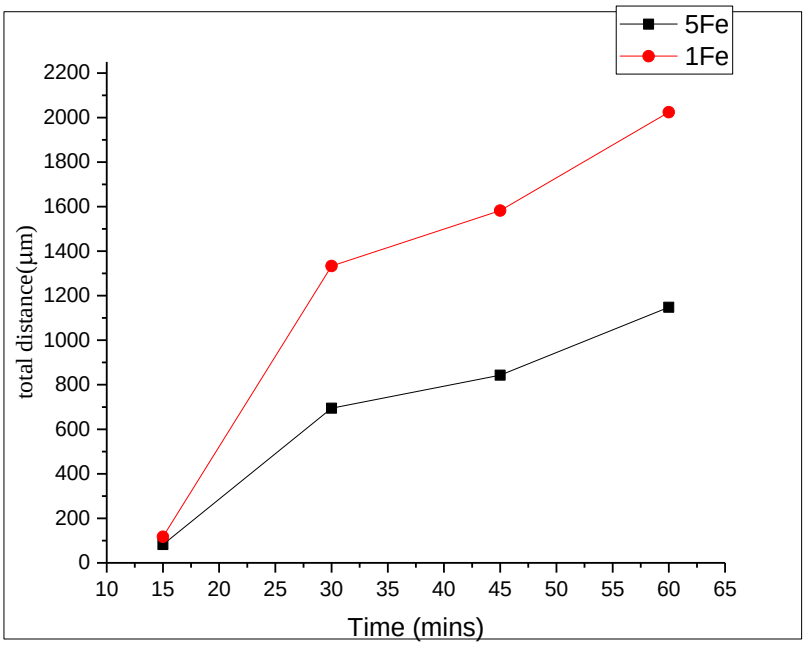

Figure 0.12. Graph showing a total reaction zone thickness against reaction time

Addition of Fe minimizes the thickness of the reaction zone, this shows that minor addition of Fe (from 1 to 5 at %) significantly reduces the growth of the reaction layer. While addition of Fe is beneficial for Ni/PbTe joints increasing Fe beyond 5at% increases the bonding temperature to which could be detrimental to inherent PbTe properties.

When Ni reacts and form telluride, Fe is not reacting and not forming any telluride so it's segregating at the grain boundary. Ni reacts and forms intermetallic while Fe left out and blocks the further reaction to occur. From the graph we can observe that after some time the Fe enriched layer will be horizontal line which shows it's not further diffusing but enriching at grain boundary

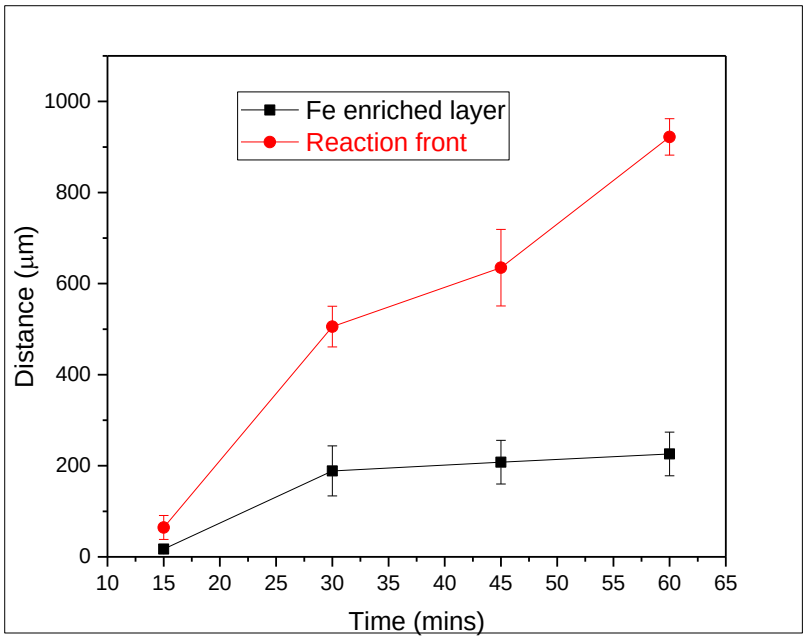

Figure 0.13. Graph showing variation of Fe enriched zone & total reaction front distance for 5at% Fe.

Annealing 0 at% Fe-Ni and 5 at % Fe- Ni/PbTe at 700 °C for 15 minutes

The following figure shows the microstructure of the sample annealed at 700 C for 15 minutes on 0 at% and 5 at % Fe-Ni/PbTe to investigate the effect of Fe addition.

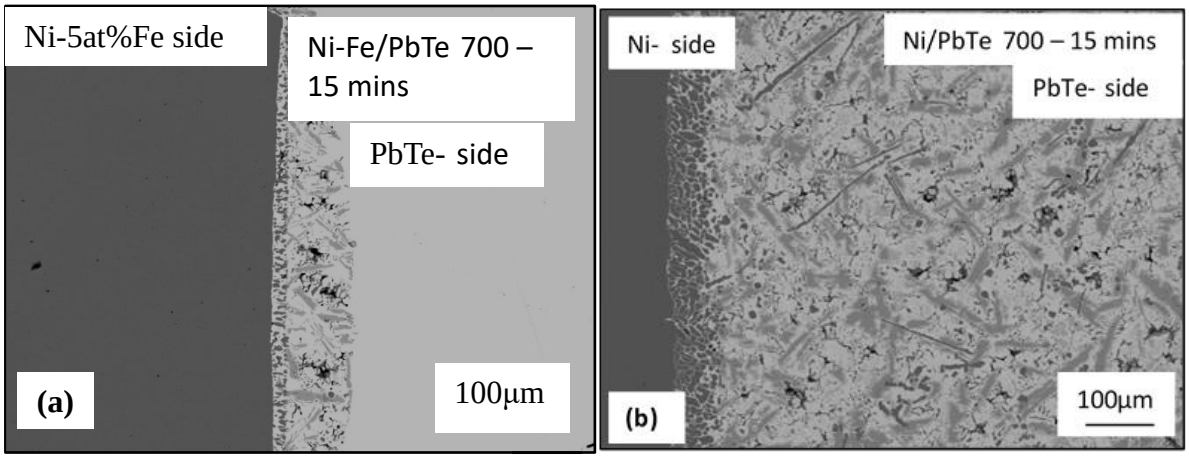

Figure 0.14. Microstructure showing a) Ni-Fe/PbTe and b) Ni/PbTe annealed at 700 °C for 15 min.

Figure 4.14. is to show how addition of Fe is affecting PbTe/ interfacial reaction fig. a) Ni-Fe/PbTe 700 – 15min which has 5at% of Fe and fig. b) is Ni/PbTe 700 – 15 min, which has 0at% of Fe. the dark contrast phase is Ni-Fe side and the white contrast phase PbTe side.in both samples Ni-Fe disc was successfully bonded to PbTe disc by diffusion bonding

technique and as we can observe from the image rapid reaction happened for the sample with 0at%Fe , PbTe side is entirely reacted while the other sample with 5at%Fe is produces clean joints which is free from interface discontinuity and porosity. The binary phase; β_2 phase, $Ni_{3\pm x}Te_2$, and ternary phase ($Ni_{50}Te_{30}Pb_{20}$) are formed for the experiments but the reaction thickness for Ni-Fe/PbTe is much less than the Ni/PbTe couple. Mostly 500 °C – 600 °C is the temperature used to fabricate bulk PbTe, in our investigation we have used up to 700 °C with contact material expected that it may affect some property of PbTe like Seebeck coefficient. In this study Seebeck coefficient is not measured, but related papers explain that there is no significant differences between the before and after the bonding. We also believe that 700 ℃ we used does not affect the Seebeck coefficient of PbTe material. The inter diffusion is the other factor that can affect the property of bulk PbTe, in this work the intermetallic formation is essential for bonding strength but too much intermetallic is not desired because it may change the chemical composition

4.4 Comparison with literature

The following table presents the comparison of the present materials systems to that of the literature reported previously.

Table 0.4. Comparison of the present materials systems to that of the literature values

TE material	Solid metal	T (°C)	Time	P (MPa)	Bonding technique	Phase formed	References
n-type PbTe	NiFeMo	700	1 hr	40	Rapid HP	Liquid Pb	[112]
n-type PbTe	Ni	600&650	1 hr	40	HP	β_2 & Ni5Pb2Te3	[115]
n-type PbTe	Ni	520	10 min	-	SPS	β_2	[117]
PbTe	Nb	700	1 hr	40	RHP	Nb_3Te_4	[108]
PbTe	Ag	400&550	50 hr	40	RHP	Ag_2Te,Pb	[3]
PbTe	FeNi	700	15 min	-	Diffusion bonding	β_2 & Ni5Pb2Te3	

C.C.Li et al.[131] studied the bonding of PbTe to Ag and Cu reporting that cu is overly diffused in the PbTe establishing the necessity of diffusion barrier between the materials. It's suggested that if the hot side temperature is kept below 400^{o}c Cu electrode can be used for a direct bond to n-type PbTe, which is very low temperature. Another material that has a closest CTE to PbTe is Ni and researchers have used as a diffusion barrier to PbTe thermoelectric materials. compering to the study Haiyang xia.et.al [115] done they observed intermetallic formation in the Ni/ PbTe joints bonded at 600^{o}c and at 650^{o}c ,a ternary phase with composition $Ni_5Pb_3Te_2$ were observed, an eutectic formation happened at the contact area with larger cracks on the Ni side. They conclude that reaction between Ni/PbTe continues during device usage and it's appropriate for low temperatures operating devices only. In our study at 600^{o}c only few Ni precipitates are observed and at 650^{o}c binary phase is observed while ternary phase is observed at 675^{o}c -1hr sample. other recent works done on PbTe mentioned above (table 1) less common electrode used for PbTe, Nb reported in [108] and Nb_3Te_4 layer mixed with Pb is observed which is weak. On the other hand; Ni, Fe and Mo alloy bonded to n-type PbTe at 700^{o}c 40MPa for 60minutes [112] . result from the aging analysis show that initial liquid penetration of Pb into the NiFeMo grains of the electrode was the cause of failure after 240 hours at 600^{o}c.C.Long et al [132] used hot pressing at 800^{o}c 50MPa and 15min for bonding n-type PbTe powder and Fe powder they reported that Fe is not suitable for n-type PbTe thermoelectric material showing the crack at the contact after the joining process. We have used Ni and Fe alloy as a diffusion barrier for PbTe thermoelectric material and its showed promising resulted prevents the reaction of Ni with PbTe which can rise the operating temperature and extend the life time of the joints. Although telluride's of Fe exist (refer to table 1), no iron telluride's were observed in this study rather enrichment of Fe was found at the grain boundaries near the interface. The thermodynamic calculations also show that no binary phase can form during the reaction of Fe with PbTe (Refer table 2)

Table 4.5 lists of formation of Gibbs free energy ($\Delta_f G_T$) of $Fe_{1.12}$ Te(β), $Fe_{0.67}$Te(δ), $FeTe_2$(Ɛ) referred from; (Barin I (1995) Thermochemical data of pure substances, 3rd edn. VCH, Weinheim and Ball RGJ, Dickinson S, Cordfunke EHP, Konings RJM (1992) Thermochemical data acquisition part 2: joint final report. The Commission of the European Communities, Brussels)[133].

Table 0.5. Table showing the Gibbs free energy of the Fe-Te systems from literature results.

Phase label	Formula in reference	Formula used here	Temperature(K)	ΔrGT(KJ/mol)
$Fe_{1.12}$ Te-β	$FeTe_{0.9}$	$Fe_{1.12}$ Te	1100	-23.458
$Fe_{0.67}$ Te-δ	$Fe_{0.67}$ Te	$Fe_{0.67}$ Te	1000	-21.610
FeTe-ε	$FeTe_2$	$Fe_{0.5}$ Te	900	-18.527

Table 4.5 illustrate that Gibbs free energy changes during formation of iron tellurides are positive at the temperatures where experiments were carried out. Our experimental results show that Fe is not reacting Therefore, Fe may not form a metallurgically bonded high strength joint with PbTe but greatly reduces the reaction of Ni in to PbTe thermoelectric element.

Table 0.6. The calculated results of the Gibbs free energy ($\Delta_r G_T$) of the reaction Fe with PbTe which is taken from literature

Chemical reaction equation	Temperature (K)	$\Delta_r G_T$(KJ/mol)
$1.12Fe + PbTe \rightarrow Fe_{1.12}Te + Pb$	1100	17.649
$0.67Fe + PbTe \rightarrow Fe_{0.67}Te + Pb$	1000	30.020
$0.5\ Fe + PbTe \rightarrow Fe_{0.5}\ Te + Pb$	900	37.540

Diffusion path

As mentioned in chapter -1 the diffusion path can be described in three ways; 1 lattice diffusion which takes place inside the lattice (interstitial and vacancy) 2, surface diffusion, and 3rd. and very important in our study is grain boundary diffusion. Grain boundaries form within the neck between individual particles as a result of random grain contacts leading to misaligned crystals. A grain boundary is essentially a collection of repeated disorientation steps. this region is not tightly packed as a region inside the grain therefore there is more open space along the grain boundary and an atom can sit in those open spaces, which allows

mass flow along with this interface. Therefore, Grain boundaries are open structure areas which act as the preferred circuit for atomic movements. At lower temperatures in metals and alloys, grain boundary diffusion is the dominant mechanism[134]. It has been shown experimentally that the jump frequency for atoms migrating along this defect is higher than that for diffusion in the lattice. And at low-temperature diffusion along these defects can be the dominant diffusion path. Diffusion along grain boundaries can be described by;

$$D_b = D_{b0} \exp - Q_b/RT$$

$$D_s > D_b > D_l$$

D_b - grain boundary diffusivity

D_{bo} – frequency factors

Q_b - the activation energy value for diffusivity

D_s and D_l are surface and lattice diffusion.

Chapter Five

5. Conclusion and Future work

5.1 Conclusion

Ni-Fe disc was successfully bonded to PbTe disc by diffusion bonding technique. Commonly researchers have used spark plasma sintering and hot pressing as a joint formation technique, which requests high temperature and pressure that may induce severe inter diffusion.

we introduced the diffusion bonding technique and it is accelerated by temperature with simple and low running coast. The process also produces clean joints which is free from interface discontinuity and porosity. The binary phase; β_2 phase, $Ni_{3\pm x}Te_2$, and ternary phase ($Ni_{50}Te_{30}Pb_{20}$) are formed at the Ni-Fe/PbTe interface while comparing with the papers that have been reported (table; 1) our result show higher temperature at which PbTe can operate. When PbTe reacts with Ni it is consumed to form Nickel telluride (β_2) but the Fe keeps on enriching the grain boundaries without reacting with PbTe. The more Ni is reacted the more Fe left out, with an increase in the time this enriched Fe, block the diffusion pathways, which inhibits movement of Ni to the PbTe side.

Initially, when Ni preferentially reacts with PbTe, Fe gets segregated at grain boundaries which retard the further movement of Ni atoms towards the interface. This reduces the availability of Ni for further reaction to happen and reduces the reaction kinetics. We conclude based on our results that Ni-5at%Fe /PbTe 700^{o}C/15min is the best one. If we increase beyond 5Fe at% it would take a longer time to join.

5.2 Future Work

The findings in this MS.C thesis are related to interface in a thermoelectric device. The optimization of joining temperature and holding time to bond lead telluride and contact material, while generating an effective and reliable interface in thermoelectric device was our goal.

Further investigation in this thesis will be;

- Studying or measuring Seebeck coefficient of bulk PbTe with Ni-Fe alloy contacts to make sure that the 700^{o}c used have no effect on the property of the PbTe thermoelectric leg.
- Measuring the thermal conductivity of the couple material (PbTe/Ni-Fe)

References

[1] "The bridge between the materials and devices of thermoelectric power generators - Energy & Environmental Science (RSC Publishing)." https://pubs.rsc.org/en/content/articlelanding/2017/ee/c6ee02488b#!divAbstract (accessed Jan. 14, 2020).

[2] K. V. Selvan, M. N. Hasan, and M. S. M. Ali, "Methodological reviews and analyses on the emerging research trends and progresses of thermoelectric generators," *International Journal of Energy Research*, Jan. 01, 2019. https://onlinelibrary.wiley.com/doi/abs/10.1002/er.4206 (accessed Jan. 15, 2020).

[3] C. C. Li *et al.*, "Silver as a highly effective bonding layer for lead telluride thermoelectric modules assembled by rapid hot-pressing," *Energy Convers. Manag.*, vol. 98, pp. 134–137, 2015.

[4] M. A. Karri, E. F. Thacher, and B. T. Helenbrook, "Exhaust energy conversion by thermoelectric generator: Two case studies," *Energy Convers. Manag.*, vol. 52, no. 3, pp. 1596–1611, 2011.

[5] S. Karabetoglu, A. Sisman, Z. F. Ozturk, and T. Sahin, "Characterization of a thermoelectric generator at low temperatures," *Energy Convers. Manag.*, vol. 62, pp. 47–50, 2012.

[6] J. He and T. M. Tritt, "Advances in thermoelectric materials research: Looking back and moving forward," *Science*, vol. 357, no. 6358, p. eaak9997, Sep. 2017, doi: 10.1126/science.aak9997.

[7] F. J. Lesage, R. Pelletier, L. Fournier, and É. V. Sempels, "Optimal electrical load for peak power of a thermoelectric module with a solar electric application," *Energy Convers. Manag.*, vol. 74, pp. 51–59, 2013.

[8] H. S. Kim, W. Liu, and Z. Ren, "The bridge between the materials and devices of thermoelectric power generators," *Energy Env. Sci*, vol. 10, no. 1, pp. 69–85, 2017, doi: 10.1039/C6EE02488B.

[9] J. R. Camargo and M. C. C. De Oliveira, "Principles of direct thermoelectric conversion," in *Heat Analysis and Thermodynamic Effects*, IntechOpen, 2011.

[10] T. M. Tritt and M. A. Subramanian, "Thermoelectric materials, phenomena, and applications: a bird's eye view," *MRS Bull.*, vol. 31, no. 3, pp. 188–198, 2006.

[11] T. M. Tritt, "Thermoelectric phenomena, materials, and applications," *Annu. Rev. Mater. Res.*, vol. 41, pp. 433–448, 2011.

[12] K. Uchida *et al.*, "Thermoelectric generation based on spin Seebeck effects," *Proc. IEEE*, vol. 104, no. 10, pp. 1946–1973, 2016.

[13] K. R. Adhikari, "Thermocouple: Facts and Theories," *Himal. Phys.*, pp. 10–14, 2017.

[14] "the seebeck coefficient of the materials mainly depends on their electron band structure which depends on the density of state (DOS) in the range of fermi level - Google Search." https://www.google.com/search?sxsrf=ACYBGNSWj6j8gdOW-o2_Ly5yFV-KF50snA%3A1580492902588&ei=Zmg0XsrOI62V4-EPwr20wAQ&q=the+seebeck+coefficient+of+the+materials+mainly+depends+on+their+electron+band+structure+which+depends+on+the+density+of+state+%28DOS%29+in+the+range+of+fermi+level&oq=the+seebeck+coefficient+of+the+materials+mainly+depends+on+their+electron+band+structure+which+depends+on+the+density+of+state+%28DOS%29+in+the+range+of+fermi+level&gs_l=psy-ab.12..0i71l8.276277.276277..278151...0.1..0.0.0.....1....2j1..gws-wiz.dIFXklxGSd8&ved=0ahUKEwjKmZ3wsq7nAhWtyjgGHcIeDUgQ4dUDCAs (accessed Feb. 01, 2020).

[15] W. Thomson, "4. on a mechanical theory of thermo-electric currents," *Proc. R. Soc. Edinb.*, vol. 3, pp. 91–98, 1857.

[16] Y. Apertet and C. Goupil, "On the fundamental aspect of the first Kelvin's relation in thermoelectricity," *Int. J. Therm. Sci.*, vol. 104, pp. 225–227, 2016.

[17] C. Gao and G. Chen, “Conducting polymer/carbon particle thermoelectric composites: Emerging green energy materials,” *Compos. Sci. Technol.*, vol. 124, pp. 52–70, 2016.
[18] G. D. Mahan, “Introduction to thermoelectrics,” *APL Mater.*, vol. 4, no. 10, p. 104806, 2016.
[19] D. Zhao and G. Tan, “A review of thermoelectric cooling: materials, modeling and applications,” *Appl. Therm. Eng.*, vol. 66, no. 1–2, pp. 15–24, 2014.
[20] B. Poudel *et al.*, “High-thermoelectric performance of nanostructured bismuth antimony telluride bulk alloys,” *Science*, vol. 320, no. 5876, pp. 634–638, 2008.
[21] D. Kraemer *et al.*, “High-performance flat-panel solar thermoelectric generators with high thermal concentration,” *Nat. Mater.*, vol. 10, no. 7, p. 532, 2011.
[22] S. B. Riffat and X. Ma, “Improving the coefficient of performance of thermoelectric cooling systems: a review,” *Int. J. Energy Res.*, vol. 28, no. 9, pp. 753–768, 2004.
[23] F. J. DiSalvo, “Thermoelectric cooling and power generation,” *Science*, vol. 285, no. 5428, pp. 703–706, 1999.
[24] Z. H. Dughaish, “Lead telluride as a thermoelectric material for thermoelectric power generation,” *Phys. B Condens. Matter*, vol. 322, no. 1, pp. 205–223, 2002, doi: https://doi.org/10.1016/S0921-4526(02)01187-0.
[25] M. Hamid Elsheikh *et al.*, “A review on thermoelectric renewable energy: Principle parameters that affect their performance,” *Renew. Sustain. Energy Rev.*, vol. 30, pp. 337–355, 2014, doi: https://doi.org/10.1016/j.rser.2013.10.027.
[26] M. Beekman, D. T. Morelli, and G. S. Nolas, “Better thermoelectrics through glass-like crystals,” *Nat. Mater.*, vol. 14, no. 12, p. 1182, 2015.
[27] B. C. Sales, “Electron crystals and phonon glasses: a new path to improved thermoelectric materials,” *MRS Bull.*, vol. 23, no. 1, pp. 15–21, 1998.
[28] G. J. Snyder, M. Christensen, E. Nishibori, T. Caillat, and B. B. Iversen, “Disordered zinc in Zn 4 Sb 3 with phonon-glass and electron-crystal thermoelectric properties,” *Nat. Mater.*, vol. 3, no. 7, p. 458, 2004.
[29] K. Takahata, Y. Iguchi, D. Tanaka, T. Itoh, and I. Terasaki, “Low thermal conductivity of the layered oxide (N a, C a) Co 2 O 4: Another example of a phonon glass and an electron crystal,” *Phys. Rev. B*, vol. 61, no. 19, p. 12551, 2000.
[30] G. S. Nolas, “Semiconductor clathrates: a PGEC system with potential for thermoelectric applications,” *MRS Online Proc. Libr. Arch.*, vol. 545, 1998.
[31] G. S. Nolas, D. T. Morelli, and T. M. Tritt, “Skutterudites: A phonon-glass-electron crystal approach to advanced thermoelectric energy conversion applications,” *Annu. Rev. Mater. Sci.*, vol. 29, no. 1, pp. 89–116, 1999.
[32] A. L. Pope, T. M. Tritt, M. A. Chernikov, and M. Feuerbacher, “Thermal and electrical transport properties of the single-phase quasicrystalline material: Al 70.8 Pd 20.9 Mn 8.3,” *Appl. Phys. Lett.*, vol. 75, no. 13, pp. 1854–1856, 1999.
[33] I. Ohkubo and T. Mori, “Anisotropic anomalies of thermoelectric transport properties and electronic structures in layered complex nitrides AMN2 (A= Na, Cu; M= Ta, Nb),” *Chem. Mater.*, vol. 27, no. 21, pp. 7265–7275, 2015.
[34] K. Mastronardi, D. Young, C.-C. Wang, P. Khalifah, R. J. Cava, and A. P. Ramirez, “Antimonides with the half-Heusler structure: New thermoelectric materials,” *Appl. Phys. Lett.*, vol. 74, no. 10, pp. 1415–1417, 1999.
[35] L.-D. Zhao *et al.*, “BiCuSeO oxyselenides: new promising thermoelectric materials,” *Energy Environ. Sci.*, vol. 7, no. 9, pp. 2900–2924, 2014.
[36] H. Alam and S. Ramakrishna, “A review on the enhancement of figure of merit from bulk to nano-thermoelectric materials,” *Nano Energy*, vol. 2, no. 2, pp. 190–212, 2013.
[37] J.-F. Li, W.-S. Liu, L.-D. Zhao, and M. Zhou, “High-performance nanostructured thermoelectric materials,” *NPG Asia Mater.*, vol. 2, no. 4, p. 152, 2010.
[38] B. C. Sales, D. Mandrus, and R. K. Williams, “Filled skutterudite antimonides: a new class of thermoelectric materials,” *Science*, vol. 272, no. 5266, pp. 1325–1328, 1996.

[39] Z.-G. Chen, G. Han, L. Yang, L. Cheng, and J. Zou, “Nanostructured thermoelectric materials: Current research and future challenge,” *Prog. Nat. Sci. Mater. Int.*, vol. 22, no. 6, pp. 535–549, 2012.
[40] A. Visconti, “Development of half-Heusler type thermoelectrical materials in a range of temperature from 300 to 500° C,” PhD Thesis, 2017.
[41] S. LeBlanc, “Thermoelectric generators: Linking material properties and systems engineering for waste heat recovery applications,” *Sustain. Mater. Technol.*, vol. 1–2, pp. 26–35, 2014, doi: https://doi.org/10.1016/j.susmat.2014.11.002.
[42] Z. Tian, S. Lee, and G. Chen, “Comprehensive review of heat transfer in thermoelectric materials and devices,” *Annu. Rev. Heat Transf.*, vol. 17, 2014.
[43] H. J. Goldsmid, “Bismuth–The Thermoelectric Material of the Future?,” in *2006 25th International Conference on Thermoelectrics*, 2006, pp. 5–10.
[44] Y. Gelbstein, Z. Dashevsky, and M. P. Dariel, “Highly efficient bismuth telluride doped p-type Pb0. 13Ge0. 87Te for thermoelectric applications,” *Phys. Status Solidi RRL–Rapid Res. Lett.*, vol. 1, no. 6, pp. 232–234, 2007.
[45] H. Fang, T. Feng, H. Yang, X. Ruan, and Y. Wu, “Synthesis and thermoelectric properties of compositional-modulated lead telluride–bismuth telluride nanowire heterostructures,” *Nano Lett.*, vol. 13, no. 5, pp. 2058–2063, 2013.
[46] I. T. Witting *et al.*, “The thermoelectric properties of bismuth telluride,” *Adv. Electron. Mater.*, vol. 5, no. 6, p. 1800904, 2019.
[47] Y. Pei, A. LaLonde, S. Iwanaga, and G. J. Snyder, “High thermoelectric figure of merit in heavy hole dominated PbTe,” *Energy Environ. Sci.*, vol. 4, no. 6, pp. 2085–2089, 2011.
[48] K. F. Hsu *et al.*, “Cubic AgPbmSbTe2+ m: bulk thermoelectric materials with high figure of merit,” *Science*, vol. 303, no. 5659, pp. 818–821, 2004.
[49] E. Quarez, K.-F. Hsu, R. Pcionek, N. Frangis, E. K. Polychroniadis, and M. G. Kanatzidis, “Nanostructuring, Compositional Fluctuations, and Atomic Ordering in the Thermoelectric Materials AgPb m SbTe2+ m. The Myth of Solid Solutions,” *J. Am. Chem. Soc.*, vol. 127, no. 25, pp. 9177–9190, 2005.
[50] T. Fu *et al.*, “Enhanced thermoelectric performance of PbTe bulk materials with figure of merit zT> 2 by multi-functional alloying,” *J. Materiomics*, vol. 2, no. 2, pp. 141–149, 2016.
[51] T. C. Harman, B. Paris, S. E. Miller, and H. L. Goering, “Preparation and some physical properties of Bi2Te3, Sb2Te3, and As2Te3,” *J. Phys. Chem. Solids*, vol. 2, no. 3, pp. 181–190, 1957.
[52] F. Hao *et al.*, “High efficiency Bi 2 Te 3-based materials and devices for thermoelectric power generation between 100 and 300 C,” *Energy Environ. Sci.*, vol. 9, no. 10, pp. 3120–3127, 2016.
[53] R. Venkatasubramanian, E. Siivola, T. Colpitts, and B. O’quinn, “Thin-film thermoelectric devices with high room-temperature figures of merit,” *Nature*, vol. 413, no. 6856, pp. 597–602, 2001.
[54] Z. Tian, S. Lee, and G. Chen, “Heat transfer in thermoelectric materials and devices,” *J. Heat Transf.*, vol. 135, no. 6, 2013.
[55] W. Li *et al.*, “High-Efficiency Skutterudite Modules at a Low Temperature Gradient,” *Energies*, vol. 12, no. 22, p. 4292, 2019.
[56] G. Chen, M. S. Dresselhaus, G. Dresselhaus, J.-P. Fleurial, and T. Caillat, “Recent developments in thermoelectric materials,” *Int. Mater. Rev.*, vol. 48, no. 1, pp. 45–66, 2003.
[57] M. Rull-Bravo, A. Moure, J. F. Fernandez, and M. Martín-González, “Skutterudites as thermoelectric materials: revisited,” *Rsc Adv.*, vol. 5, no. 52, pp. 41653–41667, 2015.
[58] M. Puyet, B. Lenoir, A. Dauscher, M. Dehmas, C. Stiewe, and E. Müller, “High temperature transport properties of partially filled Ca x Co 4 Sb 12 skutterudites,” *J. Appl. Phys.*, vol. 95, no. 9, pp. 4852–4855, 2004.

[59] M. Puyet, B. Lenoir, A. Dauscher, P. Weisbecker, and S. J. Clarke, “Synthesis and crystal structure of CaxCo4Sb12 skutterudites,” *J. Solid State Chem.*, vol. 177, no. 6, pp. 2138–2143, 2004.
[60] H. Kim, M. Kaviany, J. C. Thomas, A. Van der Ven, C. Uher, and B. Huang, “Structural order-disorder transitions and phonon conductivity of partially filled skutterudites,” *Phys. Rev. Lett.*, vol. 105, no. 26, p. 265901, 2010.
[61] T. M. Tritt, G. S. Nolas, G. A. Slack, A. C. Ehrlich, D. J. Gillespie, and J. L. Cohn, “Low-temperature transport properties of the filled and unfilled IrSb3 skutterudite system,” *J. Appl. Phys.*, vol. 79, no. 11, pp. 8412–8418, 1996.
[62] K. Wei, “Skutterudite Derivatives: A Fundamental Investigation with Potential for Thermoelectric Applications,” 2014.
[63] G. S. Nolas, G. A. Slack, D. T. Morelli, T. M. Tritt, and A. C. Ehrlich, “The effect of rare-earth filling on the lattice thermal conductivity of skutterudites,” *J. Appl. Phys.*, vol. 79, no. 8, pp. 4002–4008, 1996.
[64] C. Candolfi *et al.*, “Multiband conduction in the type-I clathrate Ba 8 Ge 43□ 3,” *Phys. Rev. B*, vol. 84, no. 20, p. 205118, 2011.
[65] K. A. Kovnir and A. V. Shevelkov, “Semiconducting clathrates: synthesis, structure and properties,” *Russ. Chem. Rev.*, vol. 73, no. 9, pp. 923–938, 2004.
[66] M. Christensen, S. Johnsen, and B. B. Iversen, “Thermoelectric clathrates of type I,” *Dalton Trans.*, vol. 39, no. 4, pp. 978–992, 2010.
[67] E. Arbelo-Jorge, “Band structure of Heusler compounds studied by photoemission and tunneling spectroscopy,” PhD Thesis, PhD thesis, Johannes Gutenberg-Universität Mainz, 2011.
[68] W. Xie, A. Weidenkaff, X. Tang, Q. Zhang, J. Poon, and T. M. Tritt, “Recent advances in nanostructured thermoelectric half-Heusler compounds,” *Nanomaterials*, vol. 2, no. 4, pp. 379–412, 2012.
[69] S. Chen and Z. Ren, “Recent progress of half-Heusler for moderate temperature thermoelectric applications,” *Mater. Today*, vol. 16, no. 10, pp. 387–395, 2013.
[70] D. Rabin, T. Kyratsi, D. Fuks, and Y. Gelbstein, “Thermoelectric transport properties of (Ti1-cAlc) NiSn half-Heusler alloy,” *Phys. Chem. Chem. Phys.*, 2020.
[71] K. Huang, Y. Yan, B. Li, Y. Li, K. Li, and J. Li, “A novel design of thermoelectric generator for automotive waste heat recovery,” *Automot. Innov.*, vol. 1, no. 1, pp. 54–61, 2018.
[72] G. J. Snyder and T. S. Ursell, “Thermoelectric efficiency and compatibility,” *Phys. Rev. Lett.*, vol. 91, no. 14, p. 148301, 2003.
[73] X. Hu *et al.*, “Power generation from nanostructured PbTe-based thermoelectrics: comprehensive development from materials to modules,” *Energy Environ. Sci.*, vol. 9, no. 2, pp. 517–529, 2016.
[74] R. A. Kishore, M. Sanghadasa, and S. Priya, “Optimization of segmented thermoelectric generator using Taguchi and ANOVA techniques,” *Sci. Rep.*, vol. 7, no. 1, pp. 1–15, 2017.
[75] “thermoelectrics.” [Online]. Available: TEGhttp://thermoelectrics.matsci.northwestern.edu/thermoelectrics/engineering.html).
[76] P. Shewmon, *Diffusion in solids*. Springer, 2016.
[77] “Diffusion Theory: Fick’s 1st Law.” https://omlc.org/classroom/ece532/class5/ficks1.html (accessed Feb. 06, 2020).
[78] “Module-5 :Diffusion,” [Online]. Available: https://omlc.org/classroom/ece532/class5/ficks1.html.
[79] “module 5 diffusion,” [Online]. Available: https://www.google.com/search?q=steady+state+diffusion&sxsrf=ALeKk034hOmRHrspgIx69ziOAFG0yQG2mA:1607693213634&source=lnms&tbm=isch&sa=X&ved=2ahUKEwi13Z_3g8btAhURuRoKHTyqAvIQ_AUoAXoECBcQAw&biw=1536&bih=722.
[80] R. J. Borg and G. J. Dienes, *An introduction to solid state diffusion*. Elsevier, 2012.

[81] J. Fage-Pedersen, “Impurity–point defect complexes: Diffusion studies in Si and SiGe, and electrical studies in Ge,” PhD Thesis, PhD thesis 2001 (www. dfi. aau. dk/∼ fage/fage-pedersen thesis. pdf), 2001.
[82] M. D. Zahari and B. Tuck, “Substitutional-interstitial diffusion in semiconductors,” *J. Phys. Appl. Phys.*, vol. 18, no. 8, p. 1585, 1985.
[83] U. M. Gosele, “Fast diffusion in semiconductors,” *Annu. Rev. Mater. Sci.*, vol. 18, no. 1, pp. 257–282, 1988.
[84] “Diffusion Movement of atoms in a material,” [Online]. Available: https://slideplayer.com/slide/3815150/.
[85] C. J. Smithells and C. E. Ransley, “The diffusion of gases through metals,” *Proc. R. Soc. Lond. Ser. -Math. Phys. Sci.*, vol. 150, no. 869, pp. 172–197, 1935.
[86] T. Katkus, “Design and construction of high temperature thermoelectric power generator module characterisation system,” 2015.
[87] C. Jiang *et al.*, “Elemental diffusion and service performance of Bi 2 Te 3-based thermoelectric generation modules with flexible connection electrodes,” *J. Electron. Mater.*, vol. 46, no. 2, pp. 1363–1370, 2017.
[88] N.-H. Bae, S. Han, K. E. Lee, B. Kim, and S.-T. Kim, “Diffusion at interfaces of micro thermoelectric devices,” *Curr. Appl. Phys.*, vol. 11, no. 5, pp. S40–S44, 2011.
[89] Y. C. Lan, D. Z. Wang, G. Chen, and Z. F. Ren, “Diffusion of nickel and tin in p-type (Bi, Sb) 2 Te 3 and n-type Bi 2 (Te, Se) 3 thermoelectric materials,” *Appl. Phys. Lett.*, vol. 92, no. 10, p. 101910, 2008.
[90] D. L. Medlin and G. J. Snyder, “Interfaces in bulk thermoelectric materials: A review for Current Opinion in Colloid and Interface Science,” *Curr. Opin. Colloid Interface Sci.*, vol. 14, no. 4, pp. 226–235, 2009, doi: https://doi.org/10.1016/j.cocis.2009.05.001.
[91] B. Song *et al.*, “The effects of diffusion barrier layers on the microstructural and electrical properties in CoSb3 thermoelectric modules,” *J. Alloys Compd.*, vol. 617, pp. 160–162, 2014.
[92] S. LeBlanc, “Thermoelectric generators: Linking material properties and systems engineering for waste heat recovery applications,” *Sustain. Mater. Technol.*, vol. 1, pp. 26–35, 2014.
[93] Q. Zhang *et al.*, “Realizing a thermoelectric conversion efficiency of 12% in bismuth telluride/skutterudite segmented modules through full-parameter optimization and energy-loss minimized integration,” *Energy Environ. Sci.*, vol. 10, no. 4, pp. 956–963, 2017.
[94] A. Muto, J. Yang, B. Poudel, Z. Ren, and G. Chen, “Skutterudite unicouple characterization for energy harvesting applications,” *Adv. Energy Mater.*, vol. 3, no. 2, pp. 245–251, 2013.
[95] D. Kraemer *et al.*, “Concentrating solar thermoelectric generators with a peak efficiency of 7.4%,” *Nat. Energy*, vol. 1, no. 11, p. 16153, 2016.
[96] A. Ziabari, E. Suhir, and A. Shakouri, “Minimizing thermally induced interfacial shearing stress in a thermoelectric module with low fractional area coverage,” *Microelectron. J.*, vol. 45, no. 5, pp. 547–553, 2014.
[97] “Weitzman: Etching bismuth telluride - Google Scholar.” https://scholar.google.com/scholar_lookup?title=Etching%20bismuth%20telluride&author=L.H.%20Weitzman&publication_year=1967 (accessed Jan. 29, 2020).
[98] “Talor PJ, Maddux JR, Meissner G, Venkatasubramanian R, Bulman G, et al.Controlled improvement in specific contact resistivity for thermoelectricmaterials by ion implantation. Appl Phys Lett 2013;103:043902 - Google Search.” https://www.google.com/search?q=Talor+PJ%2C+Maddux+JR%2C+Meissner+G%2C+Venkatasubramanian+R%2C+Bulman+G%2C+et+al.Controlled+improvement+in+specific+contact+resistivity+for+thermoelectricmaterials+by+ion+implantation.+Appl+Phys+Lett+2013%3B103%3A043902&oq=Talor+PJ%2C+Maddux+JR%2C+Meissner+G%2C+Venkatasubramanian+R%2C+Bulman+G%2C+et+al.Controlled+improvement+in+specific+contact+resistivity+for+thermoelectricmaterials+by+ion+implantation.+Appl+Phys+Lett+2013%3B103%3A043902&aqs=chrome..69i57&sourceid=chrome&ie=UTF-8 (accessed Jan. 28, 2020).

[99] “Khalatnikov: An introduction to the theory of superfluidity - Google Scholar.” https://scholar.google.com/scholar_lookup?title=Introduction%20to%20the%20theory%20of%20superfluidity&author=I.M.%20Khalatnikov&publication_year=1965 (accessed Jan. 28, 2020).
[100] “Swartz ET, Pohl RO. Thermal boundary resistance. Rev Mod Phys 1989;6 - Google Search.” https://www.google.com/search?q=Swartz+ET%2C+Pohl+RO.+Thermal+boundary+resistance.+Rev+Mod+Phys+1989%3B6&oq=Swartz+ET%2C+Pohl+RO.+Thermal+boundary+resistance.+Rev+Mod+Phys+1989%3B6&aqs=chrome..69i57&sourceid=chrome&ie=UTF-8 (accessed Jan. 28, 2020).
[101] “Sze: Physics of semiconductor devices - Google Scholar.” https://scholar.google.com/scholar_lookup?title=Physics%20of%20semiconductor%20devices&author=S.M.%20Sze&publication_year=2007 (accessed Jan. 29, 2020).
[102] O. D. Iyore *et al.*, “Interface characterization of nickel contacts to bulk bismuth tellurium selenide,” *Surf. Interface Anal. Int. J. Devoted Dev. Appl. Tech. Anal. Surf. Interfaces Thin Films*, vol. 41, no. 5, pp. 440–444, 2009.
[103] W. P. Lin, D. E. Wesolowski, and C. C. Lee, “Barrier/bonding layers on bismuth telluride (Bi2Te3) for high temperature thermoelectric modules,” *J. Mater. Sci. Mater. Electron.*, vol. 22, no. 9, pp. 1313–1320, Sep. 2011, doi: 10.1007/s10854-011-0306-0.
[104] “Using the spacegroup subpackage-ASE.” [Online]. Available: https://wiki.fysik.dtu.dk/ase/ase/spacegroup/spacegroup.html.
[105] K. Biswas *et al.*, “High-performance bulk thermoelectrics with all-scale hierarchical architectures,” *Nature*, vol. 489, no. 7416, p. 414, 2012.
[106] A. D. LaLonde, Y. Pei, and G. J. Snyder, “Reevaluation of PbTe 1- x I x as high performance n-type thermoelectric material,” *Energy Environ. Sci.*, vol. 4, no. 6, pp. 2090–2096, 2011.
[107] C. M. Jaworski and J. P. Heremans, “Thermoelectric transport properties of the n-type impurity Al in PbTe,” *Phys. Rev. B*, vol. 85, no. 3, p. 033204, 2012.
[108] H. Xia, C.-L. Chen, F. Drymiotis, A. Wu, Y.-Y. Chen, and G. J. Snyder, “Interfacial reaction between Nb foil and n-type PbTe thermoelectric materials during thermoelectric contact fabrication,” *J. Electron. Mater.*, vol. 43, no. 11, pp. 4064–4069, 2014.
[109] Z. Ren, Y. Lan, and Q. Zhang, *Advanced Thermoelectrics: Materials, Contacts, Devices, and Systems*. CRC Press, 2017.
[110] “Download citation of Junctions and diffusion barriers for high temperature thermoelectric modules,” *ResearchGate*. https://www.researchgate.net/publication/286153169_Junctions_and_diffusion_barriers_for_high_temperature_thermoelectric_modules (accessed Jan. 10, 2020).
[111] “Download citation of Thermal expansion properties of thermoelectric generating device component,” *ResearchGate*. https://www.researchgate.net/publication/4350813_Thermal_expansion_properties_of_thermoelectric_generating_device_component (accessed Jan. 10, 2020).
[112] H. Xia, F. Drymiotis, C.-L. Chen, A. Wu, Y.-Y. Chen, and G. Jeffrey Snyder, “Bonding and high-temperature reliability of NiFeMo alloy/n-type PbTe joints for thermoelectric module applications,” *J. Mater. Sci.*, vol. 50, no. 7, pp. 2700–2708, 2015, doi: 10.1007/s10853-015-8820-8.
[113] X. R. Ferreres and S. Aminorroaya Yamini, “Rapid fabrication of diffusion barrier between metal electrode and thermoelectric materials using current-controlled spark plasma sintering technique,” *J. Mater. Res. Technol.*, vol. 8, no. 1, pp. 8–13, Jan. 2019, doi: 10.1016/j.jmrt.2018.01.008.
[114] H. Xia, F. Drymiotis, C.-L. Chen, A. Wu, Y.-Y. Chen, and G. J. Snyder, “Bonding and high-temperature reliability of NiFeMo alloy/n-type PbTe joints for thermoelectric module applications,” *J. Mater. Sci.*, vol. 50, no. 7, pp. 2700–2708, 2015.

[115] H. Xia, F. Drymiotis, C.-L. Chen, A. Wu, and G. J. Snyder, “Bonding and interfacial reaction between Ni foil and n-type PbTe thermoelectric materials for thermoelectric module applications,” *J. Mater. Sci.*, vol. 49, no. 4, pp. 1716–1723, 2014.
[116] H. Xia, C.-L. Chen, F. Drymiotis, A. Wu, Y.-Y. Chen, and G. J. Snyder, “Interfacial reaction between Nb foil and n-type PbTe thermoelectric materials during thermoelectric contact fabrication,” *J. Electron. Mater.*, vol. 43, no. 11, pp. 4064–4069, 2014.
[117] X. R. Ferreres, S. A. Yamini, M. Nancarrow, and C. Zhang, “One-step bonding of Ni electrode to n-type PbTe—A step towards fabrication of thermoelectric generators,” *Mater. Des.*, vol. 107, pp. 90–97, 2016.
[118] Z. H. Dughaish and D. M. Rowe, “X-ray Identification of n-PbTe Sublimate and the Dependence.”
[119] A. Chauhan and P. Chauhan, “Powder XRD technique and its applications in science and technology,” *J Anal Bioanal Tech*, vol. 5, no. 5, pp. 1–5, 2014.
[120] V. N. E. Robinson, “Imaging with backscattered electrons in a scanning electron microscope,” *Scanning*, vol. 3, no. 1, pp. 15–26, 1980.
[121] J. I. Goldstein, D. E. Newbury, J. R. Michael, N. W. Ritchie, J. H. J. Scott, and D. C. Joy, *Scanning electron microscopy and X-ray microanalysis*. Springer, 2017.
[122] K. D. Vernon-Parry, “Scanning electron microscopy: an introduction,” *III-Vs Rev.*, vol. 13, no. 4, pp. 40–44, 2000.
[123] C. E. Lyman *et al.*, *Scanning electron microscopy, X-ray microanalysis, and analytical electron microscopy: a laboratory workbook*. Springer Science & Business Media, 2012.
[124] M. Scimeca, S. Bischetti, H. K. Lamsira, R. Bonfiglio, and E. Bonanno, “Energy Dispersive X-ray (EDX) microanalysis: A powerful tool in biomedical research and diagnosis,” *Eur. J. Histochem. EJH*, vol. 62, no. 1, 2018.
[125] “Solid-state bonding of bulk PbTe to Ni electrode... - Google Scholar.” https://scholar.google.co.in/scholar?hl=en&as_sdt=0%2C5&q=Solid-state+bonding+of+bulk+PbTe+to+Ni+electrode+for+thermoelectric+modules&btnG= (accessed Jun. 23, 2020).
[126] “Ball, R. G. J.;Dickinson, S.;Cordfunke, E. H. P.;Konings... - Google Scholar.” https://scholar.google.co.in/scholar?hl=en&as_sdt=0%2C5&q=+Ball%2C+R.+G.+J.%3BDickinson%2C+S.%3BCordfunke%2C+E.+H.+P.%3BKonings%2C+R.+J.+M.%3BDrowart%2C+J.%3BSmoes%2C+S.+%28Commission+of+the+European+Communities%2C+1992%29.+&btnG= (accessed Jun. 23, 2020).
[127] “Gulay, L. D.;Olekseyuk, I. D. Crystal structures... - Google Scholar.” https://scholar.google.co.in/scholar?hl=en&as_sdt=0%2C5&q=Gulay%2C+L.+D.%3BOlekseyuk%2C+I.+D.+Crystal+structures+of+the+compounds+Ni3Te2%2C+Ni3%E2%88%92%CE%B4Te2+%28%CE%B4%3D+0.12%29+and+Ni1.29Te.+Journal+of+alloys+and+compounds+2004%2C+376%2C+131-138.+&btnG= (accessed Jun. 23, 2020).
[128] “Kok, R. B.;Wiegers, G. A.;Jellinek, F. The system... - Google Scholar.” https://scholar.google.co.in/scholar?hl=en&as_sdt=0%2C5&q=+Kok%2C+R.+B.%3BWiegers%2C+G.+A.%3BJellinek%2C+F.+The+system+nickel%E2%80%90tellurium+I.+Structure+and+some+superstructures+of+the+Ni3%C2%B1qTe2+phase+%28preliminary+communication%29.+Recueil+des+Travaux+Chimiques+des+Pays-Bas+1965%2C+84%2C+1585-1588.+&btnG= (accessed Jun. 23, 2020).
[129] “Barstad, J., On the Tellurides of Nickel. Acta Chemica... - Google Scholar.” https://scholar.google.co.in/scholar?hl=en&as_sdt=0%2C5&q=Barstad%2C+J.%2C+On+the+Tellurides+of+Nickel.+Acta+Chemica+Scandinavica%2C+1966.+20%2810%29%3A+p.+2865-2879.&btnG= (accessed Jun. 24, 2020).
[130] “Kok, R.B., G.A. Wiegers, and F. Jellinek, The system... - Google Scholar.” https://scholar.google.co.in/scholar?hl=en&as_sdt=0%2C5&q=Kok%2C+R.B.%2C+G.A.+Wiegers%2C+and+F.+Jellinek%2C+The+system+nickel%E2%80%90tellurium+I.+Structure+and+some

+superstructures+of+the+Ni3%C2%B1qTe2+phase+%28preliminary+communication%29.+Recueil+des+Travaux+Chimiques+des+Pays-Bas%2C+1965.+84%2812%29%3A+p.+1585-1588.&btnG= (accessed Jun. 24, 2020).
[131] C. C. Li *et al.*, "Interfacial reactions between PbTe-based thermoelectric materials and Cu and Ag bonding materials," *J. Mater. Chem. C*, vol. 3, no. 40, pp. 10590–10596, 2015.
[132] C. Long, Y. Yan, J. Zhang, B. Ren, and Z. Wang, "New integration technology for PbTe element," in *2006 25th International Conference on Thermoelectrics*, 2006, pp. 386–389.
[133] I. Barin and P. Gregor, "Thermochemical data of pure substances. 3rd," *Ed. VCH*, 1995.
[134] H. Watanabe, T. Mukai, M. Kohzu, S. Tanabe, and K. Higashi, "Effect of temperature and grain size on the dominant diffusion process for superplastic flow in an AZ61 magnesium alloy," *Acta Mater.*, vol. 47, no. 14, pp. 3753–3758, 1999.